

Adaptive virtual element methods with equilibrated fluxes

F. Dassi ^{*}, J. Gedicke [†], L. Mascotto [‡]

Abstract

We present an hp -adaptive virtual element method (VEM) based on the hypercircle method of Prager and Synge for the approximation of solutions to diffusion problems. We introduce a reliable and efficient a posteriori error estimator, which is computed by solving an auxiliary global mixed problem. We show that the mixed VEM satisfies a discrete inf-sup condition, with inf-sup constant independent of the discretization parameters. Furthermore, we construct a stabilization for the mixed VEM, with explicit bounds in terms of the local degree of accuracy of the method. The theoretical results are supported by several numerical experiments, including a comparison with the residual a posteriori error estimator. The numerics exhibit the p -robustness of the proposed error estimator. In addition, we provide a first step towards the localized flux reconstruction in the virtual element framework, which leads to an additional reliable a posteriori error estimator that is computed by solving local (cheap-to-solve and parallelizable) mixed problems. We provide theoretical and numerical evidence that the proposed local error estimator suffers from a lack of efficiency.

AMS subject classification: 65N12, 65N30, 65N50.

Keywords: virtual element method, hypercircle method, equilibrated fluxes, hp -adaptivity, polygonal meshes

1 Introduction

Polygonal/polyhedral methods have several advantages over more standard technologies based on triangular/tetrahedral meshes. For instance, when refining a mesh adaptively, the use of general shaped elements allows for the presence of hanging nodes and interfaces. This simplifies the construction of hierarchies of meshes. Amongst the various polytopal methods, the virtual element method (VEM) has received an increasing attention over the last years; see [5].

Adaptivity in the VEM has been applied to several problems: general elliptic problems in primal [11, 15, 22] and mixed formulation [24], Steklov eigenvalue problems [44], the elasticity equations [43], the hp -version of the VEM [12], recovery-based VEM [28], superconvergent gradient recovery [37], discrete fracture network flow simulations [16], parabolic problems with moving meshes [23], and anisotropic discretizations [1, 50]. In all these references, residual error estimators were analyzed, whereas equilibrated error estimators have not been investigated so far.

The hypercircle method for the computation of equilibrated error estimators was introduced by Prager and Synge in [46]; see also [2]. The idea behind it consists in constructing an error estimator based on the approximations of the primal *and* the mixed formulations of the problem. In the finite element framework, a combined error of the primal and mixed formulations is equal to a term involving the gradient of the solution to the primal method *and* the equilibrated flux solution to the mixed method, up to oscillation terms.

Braess and Schöberl [19], and later Ern and Vohralík [35] provided a major improvement to the hypercircle method. They designed an error estimator based on equilibrated fluxes using the solution to the primal method and a combination of discrete solutions to local (cheap-to-solve and parallelizable) mixed problems.

In the seminal works [18, 19], Braess, Schöberl, and collaborators proved that the equilibrated error estimator is reliable and efficient also in terms of the polynomial degree p . As discussed

^{*}Dip. di Matematica e Applicazioni, Università degli Studi di Milano-Bicocca, Italy (franco.dassi@unimib.it)

[†]Institut für Numerische Simulation, Universität Bonn, 53115 Bonn (gedicke@ins.uni-bonn.de)

[‡]Fakultät für Mathematik, Universität Wien, 1090 Vienna, Austria (lorenzo.mascotto@univie.ac.at)

by Melenk and Wohlmuth [40, Theorem 3.6], this is not the case for the residual error estimator. The p -robustness of the equilibrated error estimator is proven in the discontinuous Galerkin (dG) setting as well; see, e.g., [35] and the references therein. Hence, they are very well suited for hp -adaptivity; see, e.g., [33].

Local flux reconstruction techniques have been applied to various problems, e.g., parabolic problems [34], reaction diffusion problems [48], the Helmholtz equation [27, 29] and magnetostatic problems [36].

This paper represents the first attempt to combine the hypercircle method with the VEM. In particular, we want to dovetail the geometric flexibility of the VEM with the robustness properties of the hypercircle method and the flux reconstruction. We analyze the hypercircle method for the h -, p -, and hp -versions of the VEM.

The structure and contents of the paper are as follows. In Section 2, we introduce the VEM for the primal and mixed formulations of a two dimensional diffusion problem. Despite the construction of the two methods is well understood [5, 7, 21], there are two issues that we want to address, which have not been covered in the literature so far. We show that

- the mixed formulation of the VEM satisfies an inf-sup condition, with inf-sup constant independent of the degree of accuracy of the method;
- we construct a stabilization of the mixed VEM, with stability bounds that are explicit in terms of such degree of accuracy.

In Section 3, we introduce an equilibrated error estimator, and we prove its reliability and efficiency. Such error estimator consists of two terms. One is similar to the FEM equilibrated error estimator; the other involves two stabilization terms, typical of the VEM framework. Numerical experiments are presented in Section 4. Amongst them, we show that the proposed error estimator is p -robust, differently from the residual error estimator of [12]. Moreover, we display the performance of the h - and of the hp -hypercircle method, based on the Melenk-Wohlmuth's hp -refining strategy presented in [40].

In Section 5, we present a first step towards the analysis of local flux reconstruction in the VEM framework. Here, we discuss how to design a reliable error estimator, using local VE flux reconstructions. Amongst the various technical tools needed in the analysis, we provide

- the design of a high-order virtual element partition of unity, which differs from the standard one introduced in [13, 45];
- the design of local mixed VEM, satisfying an equilibration condition on fluxes and a residual-type equation.

Numerical results with this new error estimator are the topic of Section 6. Here, we check that the equilibration condition is fulfilled, which guarantees reliability. However, notably for high-order methods, we have theoretical and numerical evidence that the local error estimator suffers from a lack of efficiency. This paves the way to future studies, where a deeper analysis on the design of local mixed problems has to be performed. We draw some conclusions in Section 7.

Notation. Throughout the paper, we employ a standard notation for Sobolev spaces. Given a measurable open set $D \subset \mathbb{R}^2$ and $s \in \mathbb{N}$, $L^2(D)$ and $H^s(D)$ denote the standard Lebesgue and Sobolev spaces endowed with inner products $(\cdot, \cdot)_{s,D}$ and seminorms $|\cdot|_{s,D}$. We set the Sobolev norm of order s as

$$\|\cdot\|_{s,D}^2 := \sum_{\ell=0}^s \|\cdot\|_{\ell,D}^2.$$

The case $s = 1$ is special and, when no confusion occurs, we will write

$$a^D(\cdot, \cdot) = (\cdot, \cdot)_{1,D}.$$

We define fractional order Sobolev spaces via interpolation theory [49], whereas we define Sobolev negative order spaces by duality as

$$H^{-1}(D) := [H_0^1(D)]^*, \quad H^{-\frac{1}{2}}(\partial D) := [H^{\frac{1}{2}}(\partial D)]^*,$$

and endow them with the norms

$$\|v\|_{-1,D} := \sup_{w \in H_0^1(D), w \neq 0} \frac{(v, w)_{0,D}}{|w|_{1,D}}, \quad \|v\|_{-\frac{1}{2}, \partial D} := \sup_{w \in H^{\frac{1}{2}}(\partial D), w \neq 0} \frac{(v, w)_{0, \partial D}}{\|w\|_{\frac{1}{2}, \partial D}}. \quad (1)$$

Recall the definition of the differential operators

$$\operatorname{div} = \partial_x + \partial_y, \quad \operatorname{rot} = \partial_y - \partial_x.$$

and introduce the $H(\operatorname{div})$ and $H(\operatorname{rot})$ spaces

$$H(\operatorname{div}, D) := \{\boldsymbol{\tau} \in [L^2(D)]^2 \mid \operatorname{div}(\boldsymbol{\tau}) \in L^2(D)\}, \quad H(\operatorname{rot}, D) := \{\boldsymbol{\tau} \in [L^2(D)]^2 \mid \operatorname{rot}(\boldsymbol{\tau}) \in L^2(D)\}.$$

For all $\ell \in \mathbb{N}$, $\mathbb{P}_\ell(D)$ denotes the space of polynomials of degree at most ℓ over D . We will employ multi-indices $\boldsymbol{\alpha} \in \mathbb{N}^2$ to describe the basis elements of $\mathbb{P}_\ell(D)$. To this purpose, we will use the natural bijection $\mathbb{N} \leftrightarrow \mathbb{N}_0^2$ given by

$$1 \leftrightarrow (0, 0), \quad 2 \leftrightarrow (1, 0), \quad 3 \leftrightarrow (0, 1), \quad 4 \leftrightarrow (2, 0), \quad 5 \leftrightarrow (1, 1), \quad 6 \leftrightarrow (0, 2), \quad \dots \quad (2)$$

As a matter of style, we employ the following notation. Given two positive quantities a and b , we write $a \lesssim b$ if there exists a positive constant C such that $a \leq Cb$. We write $a \approx b$ if $a \lesssim b$ and $b \lesssim a$ are valid at the same time.

The model problem. Let $\Omega \subset \mathbb{R}^2$ be a polygonal domain with boundary $\partial\Omega$ split into $\partial\Omega = \Gamma_D \cup \Gamma_N$ with $\Gamma_D \neq \emptyset$ and $\Gamma_D \cap \Gamma_N = \emptyset$. Denote the outward unit normal vector on Γ_N by \mathbf{n} . Let \mathbb{K} be a smooth scalar function such that there exist two positive constants $k_* < k^*$ satisfying

$$0 < k_* \leq \mathbb{K}(\mathbf{x}) \leq k^* < +\infty \quad \text{for almost all } \mathbf{x} \in \Omega. \quad (3)$$

The primal formulation. Let $f \in L^2(\Omega)$, $g_D \in H^{\frac{1}{2}}(\Gamma_D)$, and $g_N \in H^{-\frac{1}{2}}(\Gamma_N)$. We aim to approximate the solution to the problem: find \tilde{u} such that

$$\begin{cases} -\operatorname{div}(\mathbb{K} \nabla \tilde{u}) = f & \text{in } \Omega \\ \tilde{u} = g_D & \text{on } \Gamma_D \\ \mathbf{n} \cdot (\mathbb{K} \nabla \tilde{u}) = g_N & \text{on } \Gamma_N. \end{cases} \quad (4)$$

Define spaces

$$\tilde{V}_{g_D} := \{\tilde{v} \in H^1(\Omega) \mid \tilde{v} = g_D \text{ on } \Gamma_D\}, \quad \tilde{V}_0 := \{\tilde{v} \in H^1(\Omega) \mid \tilde{v} = 0 \text{ on } \Gamma_D\},$$

and bilinear form

$$\tilde{a}(\tilde{u}, \tilde{v}) := (\mathbb{K} \nabla \tilde{u}, \nabla \tilde{v})_{0,\Omega} \quad \forall \tilde{u}, \tilde{v} \in H^1(\Omega). \quad (5)$$

The weak formulation of problem (4) reads

$$\begin{cases} \text{find } \tilde{u} \in \tilde{V}_{g_D} \text{ such that} \\ \tilde{a}(\tilde{u}, \tilde{v}) = (f, \tilde{v})_{0,\Omega} + (g_N, \tilde{v})_{0,\Gamma_N} \quad \forall \tilde{v} \in \tilde{V}_0. \end{cases} \quad (6)$$

Term $(g_N, \tilde{v})_{0,\Gamma_N}$ has to be understood as a duality pairing between $H^{-\frac{1}{2}}(\Gamma_N)$ and $H^{\frac{1}{2}}(\Gamma_N)$.

The mixed formulation. Define spaces

$$\begin{aligned} \boldsymbol{\Sigma}_{g_N} &:= \{\boldsymbol{\tau} \in H(\operatorname{div}, \Omega) \mid \mathbf{n} \cdot \boldsymbol{\tau} = g_N \text{ on } \Gamma_N\}, \\ \boldsymbol{\Sigma}_0 &:= \{\boldsymbol{\tau} \in H(\operatorname{div}, \Omega) \mid \mathbf{n} \cdot \boldsymbol{\tau} = 0 \text{ on } \Gamma_N\}, \quad V := L^2(\Omega), \end{aligned}$$

and bilinear forms

$$\begin{aligned} a(\boldsymbol{\sigma}, \boldsymbol{\tau}) &:= \int_{\Omega} \mathbb{K}^{-1} \boldsymbol{\sigma} \cdot \boldsymbol{\tau} \quad \forall \boldsymbol{\sigma}, \boldsymbol{\tau} \in H(\operatorname{div}, \Omega), \\ b(\boldsymbol{\tau}, v) &:= - \int_{\Omega} \operatorname{div}(\boldsymbol{\tau}) v \quad \forall \boldsymbol{\tau} \in H(\operatorname{div}, \Omega), \forall v \in V. \end{aligned} \quad (7)$$

We point out that \tilde{V}_{g_D} and Σ_{g_N} are not vector spaces in general.

Consider the mixed formulation of problem (6). In strong formulation, it consists in finding σ and u such that

$$\begin{cases} \mathbb{K}^{-1}\sigma = -\nabla u & \text{in } \Omega \\ \operatorname{div}(\sigma) = f & \text{in } \Omega \\ u = g_D & \text{on } \Gamma_D \\ \sigma = -g_N & \text{on } \Gamma_N, \end{cases}$$

whereas, in weak formulation, it reads

$$\begin{cases} \text{find } (\sigma, u) \in \Sigma_{g_N} \times V \text{ such that} \\ a(\sigma, \tau) + b(\tau, u) = -(g_D, \mathbf{n} \cdot \tau)_{0, \Gamma_D} \quad \forall \tau \in \Sigma_0 \\ b(\sigma, v) = (-f, v)_{0, \Omega} \quad \forall v \in V. \end{cases} \quad (8)$$

The term $(g_D, \mathbf{n} \cdot \tau)_{0, \Gamma_D}$ has to be understood as a duality pairing between $H^{\frac{1}{2}}(\Gamma_D)$ and $H^{-\frac{1}{2}}(\Gamma_D)$.

The well-posedness of (6) and (8) is a consequence of Lax-Milgram lemma and of standard inf-sup theory; see, e.g., [17].

Remark 1. Formulations (6) and (8) are equivalent. Moreover, given their solutions \tilde{u} and τ , the following identity is valid:

$$\nabla \tilde{u} = -\mathbb{K}^{-1}\sigma. \quad (9)$$

Remark 2. As a matter of style, we will employ the following notation in the remainder of the paper. We will use a \sim whenever referring to functions, spaces, etc. associated with the primal formulation. No \sim is employed as for the mixed formulation.

2 Virtual element discretization

In this section, we introduce the VEM for both primal (6) and mixed (8) formulations. More precisely, we introduce the notation and certain assumptions for the polygonal meshes and the data of the problems in Section 2.1. Next, we describe the virtual element methods for the discretization of the primal (6) and mixed (8) formulations in Sections 2.2 and 2.3, respectively. Section 2.4 deals with the construction of explicit stabilizations, whereas we prove the well-posedness of the two methods in Section 2.5.

2.1 Polygonal meshes

Consider $\{\mathcal{T}_n\}_{n \in \mathbb{N}}$ a sequence of decompositions of Ω into polygons with straight edges. Hanging nodes are dealt with as standard nodes. Given a mesh \mathcal{T}_n , we denote its set of vertices, boundary vertices, and internal vertices by \mathcal{V}_n , \mathcal{V}_n^B , and \mathcal{V}_n^I , respectively. Furthermore, we denote its set of edges, boundary edges, and internal edges by \mathcal{E}_n , \mathcal{E}_n^B , and \mathcal{E}_n^I , respectively.

To each $K \in \mathcal{T}_n$, we associate \mathcal{V}^K its set of vertices and \mathcal{E}^K its set of edges. We denote its diameter and its centroid by h_K and \mathbf{x}_K . Finally, for all edges $e \in \mathcal{E}_n$, we fix once and for all \mathbf{n}_e , the unit normal vector associated with e and we denote the length of e by h_e .

For all $n \in \mathbb{N}$, \mathcal{T}_n is a conforming polygonal decomposition, i.e., every internal edge belongs to the intersection of the boundary of two neighbouring elements. Also, \mathcal{T}_n is conforming with respect to the Dirichlet and Neumann boundaries. In other words, for all boundary edges $e \in \mathcal{E}_n^B$, either $e \subset \Gamma_D$ or $e \subset \Gamma_N$.

We assume the following properties on the meshes and on the data of problems (6) and (8): for all $n \in \mathbb{N}$,

- (G1) every $K \in \mathcal{T}_n$ is star-shaped with respect to a ball of radius greater than or equal to γh_K , for some positive constant γ ;
- (G2) given $K \in \mathcal{T}_n$, for all its edges $e \in \mathcal{E}^K$, h_K is smaller than or equal to $\tilde{\gamma} h_e$, for some positive constant $\tilde{\gamma}$;
- (K) diffusion parameter \mathbb{K} is piecewise constant over $\{\mathcal{T}_n\}_n$;

(D) boundary data g_D and g_N are piecewise polynomials of a given degree $p \in \mathbb{N}$ over Γ_D and Γ_N .

We employ assumptions (G1) and (G2) in the analysis of the forthcoming sections. Instead, we call for assumptions (K) and (D) to simplify the analysis. When no confusion occurs, we denote the piecewise divergence operator over \mathcal{T}_n by div .

Assumptions (G1)–(G2) can be generalized [10, 20, 25]. We stick to the current setting for the sake of simplicity.

2.2 Virtual elements for the primal formulation

Here, we introduce the virtual element discretization of problem (6), mimicking what is done in [7]. We assume that degree of accuracy $p \in \mathbb{N}$ is uniform over all the elements; see Remark 3 below for the variable degree case.

Virtual element spaces. Given an element $K \in \mathcal{T}_n$, we define the local nodal virtual element space on K as

$$\tilde{V}_n(K) := \{\tilde{v}_n \in C^0(\overline{K}) \mid \tilde{v}_n|_e \in \mathbb{P}_p(e) \text{ for all } e \in \mathcal{E}^K, \quad \Delta \tilde{v}_n \in \mathbb{P}_{p-2}(K)\}.$$

We observe that $\mathbb{P}_p(K) \subseteq \tilde{V}_n$. Further, the functions in \tilde{V}_n are available in closed form on ∂K but not in K .

Given multi-indices α as in bijection (2), let $\{m_\alpha^K\}_{|\alpha|=0}^{p-2}$ be any basis of $\mathbb{P}_{p-2}(K)$. We assume that basis elements m_α^K are invariant with respect to dilations and translations. Let $\tilde{v}_n \in \tilde{V}_n(K)$. Consider the following set of linear functionals:

- the point values of \tilde{v}_n at the vertices of K ;
- the point values of \tilde{v}_n at the $p-1$ internal Gauss-Lobatto nodes of each edge of K ;
- (scaled) moments

$$\frac{1}{|K|} \int_K \tilde{v}_n m_\alpha^K \quad \forall |\alpha| = 0, \dots, p-2. \quad (10)$$

We are going to discuss possible choices of the polynomial basis in Section 4 and 6.

Proposition 2.1. *For all $K \in \mathcal{T}_n$, the above set of linear functionals is a set of unisolvent degrees of freedom for $\tilde{V}_n(K)$.*

Proof. See [7, Section 4.1]. □

The global virtual element space with no boundary conditions is obtained by merging the local spaces continuously:

$$\tilde{V}_n := \left\{ \tilde{v}_n \in C^0(\overline{\Omega}) \mid \tilde{v}_n|_K \in \tilde{V}_n(K) \quad \forall K \in \mathcal{T}_n \right\}.$$

We incorporate the Dirichlet boundary conditions in the space by imposing the degrees of freedom associated with the edges in Γ_D . We define discrete trial and test spaces

$$\begin{aligned} \tilde{V}_{n,g_D} &:= \left\{ \tilde{v}_n \in \tilde{V}_n \mid v_n = g_D \text{ on } e \text{ if } e \subset \Gamma_D \right\}, \\ \tilde{V}_{n,0} &:= \left\{ \tilde{v}_n \in \tilde{V}_n \mid v_n = 0 \text{ on } e \text{ if } e \subset \Gamma_D \right\}. \end{aligned}$$

We associate a set of unisolvent degrees of freedom, obtained by an H^1 -conforming coupling of their local counterparts, with each global space.

Projectors. For all $K \in \mathcal{T}_n$, by means of the degrees of freedom, we can compute the local H^1 projector $\tilde{\Pi}_p^\nabla : \tilde{V}_n(K) \rightarrow \mathbb{P}_p(K)$ defined as

$$\tilde{a}^K(\tilde{v}_n - \tilde{\Pi}_p^\nabla \tilde{v}_n, q_p) = 0 \quad \forall q_p \in \mathbb{P}_p(K), \quad \int_{\partial K} (\tilde{v}_n - \tilde{\Pi}_p^\nabla \tilde{v}_n) = 0 \quad \forall \tilde{v}_n \in \tilde{V}_n. \quad (11)$$

Furthermore, for all $K \in \mathcal{T}_n$ and for all $p \geq 2$, we introduce the local $L^2(K)$ projector $\tilde{\Pi}_{p-2}^0 : \tilde{V}_n(K) \rightarrow \mathbb{P}_{p-2}(K)$ defined as

$$(\tilde{v}_n - \tilde{\Pi}_{p-2}^0 \tilde{v}_n, q_{p-2})_{0,K} = 0 \quad \forall \tilde{v}_n \in \tilde{V}_n(K), \quad \forall q_{p-2} \in \mathbb{P}_{p-2}(K).$$

This projector is computable via bubble degrees of freedom (10).

Discrete bilinear forms and right-hand side. Functions in \tilde{V}_n are known on the skeleton of the mesh only. Consequently, for all \tilde{u}_n and \tilde{v}_n belonging to \tilde{V}_n , it is not possible to compute bilinear form $\tilde{a}(\tilde{u}_n, \tilde{v}_n)$ (5) explicitly. Thence, following the VEM gospel [7], we split global bilinear form $\tilde{a}(\cdot, \cdot)$ into a sum of local contributions:

$$\tilde{a}(\tilde{u}, \tilde{v}) = \sum_{K \in \mathcal{T}_n} \int_K \mathbb{K} \nabla \tilde{u} \cdot \nabla \tilde{v} =: \sum_{K \in \mathcal{T}_n} \tilde{a}^K(\tilde{u}|_K, \tilde{v}|_K) \quad \forall \tilde{u}, \tilde{v} \in \tilde{V}.$$

We allow for the following variational crime in the design of the local bilinear form. Let $\tilde{S}^K : \ker(\tilde{\Pi}_p^\nabla) \times \ker(\tilde{\Pi}_p^\nabla) \rightarrow \mathbb{R}$ be any bilinear form computable via the degrees of freedom and satisfying

$$\tilde{\alpha}_* \tilde{a}^K(\tilde{v}_n, \tilde{v}_n) \leq \tilde{S}^K(v_n, v_n) \leq \tilde{\alpha}^* \tilde{a}^K(\tilde{v}_n, \tilde{v}_n) \quad \forall K \in \mathcal{T}_n, \quad \forall \tilde{v}_n \in \ker(\tilde{\Pi}_p^\nabla). \quad (12)$$

Constants $0 < \tilde{\alpha}_* \leq \tilde{\alpha}^* < +\infty$ depend possibly on the geometry of the polygonal decomposition, on degree of accuracy p , and on \mathbb{K} , but must be independent of h_K .

Introducing local discrete bilinear forms

$$\tilde{a}_n^K(\tilde{u}_n, \tilde{v}_n) := (\mathbb{K} \nabla \tilde{\Pi}_p^\nabla \tilde{u}_n, \nabla \tilde{\Pi}_p^\nabla \tilde{v}_n) + \tilde{S}^K((I - \tilde{\Pi}_p^\nabla) \tilde{u}_n, (I - \tilde{\Pi}_p^\nabla) \tilde{v}_n) \quad \forall \tilde{u}_n, \tilde{v}_n \in \tilde{V}_n(K),$$

we define global discrete bilinear form

$$\tilde{a}_n(\tilde{u}_n, \tilde{v}_n) := \sum_{K \in \mathcal{T}_n} \tilde{a}_n^K(\tilde{u}_n|_K, \tilde{v}_n|_K) \quad \forall \tilde{u}_n, \tilde{v}_n \in \tilde{V}_n.$$

As discussed in [5], bilinear form $\tilde{a}_n(\cdot, \cdot)$ is coercive with constant $\min(k_*, \min_{K \in \mathcal{T}_n} \tilde{\alpha}_*)$ and continuous with constant $\max(k^*, \max_{K \in \mathcal{T}_n} \tilde{\alpha}^*)$. Explicit choices of stabilization (12) are detailed in Section 2.4.

As for the treatment of the right-hand side in the case $p = 1$, we refer the reader to [5] for details, whilst, for $p \geq 2$, we approximate the right-hand side $(f, v)_{0,\Omega}$ perpetrating the following variational crime:

$$\langle f, \tilde{v}_n \rangle_n := \sum_{K \in \mathcal{T}_n} \langle f, \tilde{v}_n|_K \rangle_{n,K} := \sum_{K \in \mathcal{T}_n} (f, \tilde{\Pi}_{p-2}^0 v_n|_K)_{0,K} \quad \forall v_n \in \tilde{V}_n.$$

The virtual element method for the primal formulation. The virtual element method tailored for the approximation of the problem in primal formulation (6) reads

$$\begin{cases} \text{find } \tilde{u}_n \in \tilde{V}_{n,g_D} \text{ such that} \\ \tilde{a}_n(\tilde{u}_n, v) = \langle f, \tilde{v}_n \rangle_n + (g_N, \tilde{v}_n)_{0,\Gamma_N} \quad \forall \tilde{v}_n \in \tilde{V}_{n,0}. \end{cases} \quad (13)$$

Remark 3. So far, we have discussed the construction of virtual elements with uniform degree of accuracy over all the elements. Indeed, the flexibility of the virtual element framework allows for the construction of global spaces with variable degrees of accuracy. Let \mathcal{T}_n be a mesh with $N_{\mathcal{T}_n}$ elements. Consider $\mathbf{p} \in \mathbb{N}^{N_{\mathcal{T}_n}}$ and associate to each $K \in \mathcal{T}_n$ a degree of accuracy p_K . To each internal edge, we associate the maximum of the degrees of accuracy of the two neighbouring elements, whereas, to each boundary edge, we associate the degree of accuracy of the only neighbouring element. The definition and cardinality of the bulk and edge degrees of freedom is performed accordingly. We refer to [8, Section 3] for a thorough presentation of the variable degree virtual element spaces case. ■

2.3 Virtual elements for the mixed formulation

In this section, we discuss the virtual element discretization of mixed formulation (8); see also [21]. For the case of piecewise analytic diffusivity tensor \mathbb{K} , we refer the reader to [6, 7]. We consider a uniform degree of accuracy $p \in \mathbb{N}$ over all the elements; see Remark 5 below for the variable degree of accuracy case.

Virtual element spaces. We define the virtual element spaces for both the primal and for the flux variables. As for the primal variable space, we define $V_n \subset V$ as the space of piecewise discontinuous polynomials of degree $p - 1$ over \mathcal{T}_n , i.e.,

$$V_n := \mathcal{S}^{p-1, -1}(\Omega, \mathcal{T}_n).$$

Given multi-indices α as in bijection (2), let $\{m_\alpha^K\}_{|\alpha|=0}^{p-1}$ be any basis of $\mathbb{P}_{p-1}(K)$. We assume that basis elements m_α^K are invariant with respect to dilations and translations. A set of unisolvent degrees of freedom is provided by scaled moments: given $v_n \in V_n(K)$,

$$\frac{1}{|K|} \int_K v_n m_\alpha^K \quad \forall |\alpha| = 0, \dots, p-1.$$

The construction of the flux spaces is as follows. On each element K , we define local space

$$\Sigma_n(K) := \left\{ \tau_n \in H(\operatorname{div}, K) \cap H(\operatorname{rot}, K) \mid \mathbf{n} \cdot \tau_n|_e \in \mathbb{P}_p(e) \text{ for all } e \in \mathcal{E}^K, \right. \\ \left. \operatorname{div}(\tau_n) \in \mathbb{P}_{p-1}(K), \operatorname{rot}(\tau_n) \in \mathbb{P}_{p-1}(K) \right\}. \quad (14)$$

Observe that $[\mathbb{P}_p(K)]^2 \subseteq \Sigma_n(K)$ and that functions in $\Sigma_n(K)$ are not known in closed form on ∂K nor inside element K .

For all $p \in \mathbb{N}$, define

$$\mathcal{G}_p(K) := \nabla \mathbb{P}_{p+1}(K).$$

For all $K \in \mathcal{T}_n$, let $\{\mathbf{m}_\alpha^K\}_{\alpha=1}^{\dim(\mathcal{G}_p(K))}$ be a basis of $\mathcal{G}_p(K)$. We assume that basis elements \mathbf{m}_α^K are invariant with respect to dilations and translations. An explicit construction of the basis for polynomial space $\mathcal{G}_p(K)$ can be found, e.g., in [32, Proposition 2.1]. Further, introduce $\{m_\alpha^K\}_{|\alpha|=0}^p$, a basis of $\mathbb{P}_p(K)$. We assume that the basis elements are invariant with respect to dilations and translations.

Consider the following set of linear functionals: given $\tau_n \in \Sigma_n(K)$,

- for all edges $e \in \mathcal{E}^K$, the evaluation at the $p + 1$ Gauss nodes $\{\nu_j^e\}_{j=0}^p$ of e

$$(\mathbf{n} \cdot \tau_n)(\nu_j) \quad \forall j = 0, \dots, p; \quad (15)$$

- the gradient-like moments

$$\frac{1}{|K|} \int_K \tau_n \cdot \mathbf{m}_\alpha^K \quad \forall \alpha = 1, \dots, \dim(\mathcal{G}_{p-2}(K)); \quad (16)$$

- the rotor-like moments

$$\frac{h_K}{|K|} \int_K \operatorname{rot}(\tau_n) m_\alpha^K \quad \forall |\alpha| = 0, \dots, p-1. \quad (17)$$

Proposition 2.2. *The set of linear functionals in (15)–(17) is a set of unisolvent degrees of freedom for $\Sigma_n(K)$, for all $K \in \mathcal{T}_n$.*

Proof. Since the dimension of $\Sigma_n(K)$ equals the number of linear functionals (15)–(17), it is enough to show that given $\tau_n \in \Sigma_n$ with functionals equals to zero is zero. In particular, we show that τ_n solves a div-rot problem with zero data.

Clearly, we have $\tau_n|_{\partial K} = 0$, thanks to boundary degrees of freedom (15). Moreover, $\operatorname{div}(\tau_n) = 0$. In fact, thanks to the definition of degrees of freedom (15)–(16), an integration by parts yields

$$\int_K \operatorname{div}(\tau_n) q_{p-1} = - \int_K \tau_n \cdot \nabla q_{p-1} + \int_{\partial K} \tau \cdot \mathbf{n} q_{p-1} = 0 \quad \forall q_{p-1} \in \mathbb{P}_{p-1}(K).$$

Eventually, thanks to rotor moments (17), we get $\operatorname{rot}(\tau_n) = 0$. \square

Define the jump operator $[[\cdot]]_e$ across an edge e as follows. If e is an internal edge shared by the elements K_1 and K_2 with outward unit normal vectors \mathbf{n}_{K_1} and \mathbf{n}_{K_2} , respectively, and given \mathbf{n}_e the global unit normal vector associated with e , set

$$[[\boldsymbol{\sigma}_n]]_e = (\mathbf{n}_e \cdot \mathbf{n}_{K_1})\mathbf{n}_e \cdot \boldsymbol{\sigma}_{K_1} + (\mathbf{n}_e \cdot \mathbf{n}_{K_2})\mathbf{n}_e \cdot \boldsymbol{\sigma}_{K_2}.$$

Instead, if e is a boundary edge, set $[[\boldsymbol{\sigma}_n]]_e = \mathbf{n}_e \cdot \boldsymbol{\sigma}_n$.

We define global space $\boldsymbol{\Sigma}_n$ without boundary conditions, by coupling the normal components at the internal interfaces between elements:

$$\boldsymbol{\Sigma}_n := \{ \boldsymbol{\sigma}_n \in H(\operatorname{div}, \Omega) \mid \boldsymbol{\sigma}_n|_K \in \boldsymbol{\Sigma}_n(K) \ \forall K \in \mathcal{T}_n, \quad [[\boldsymbol{\sigma}_n]]_e = 0 \ \forall e \in \mathcal{E}_n^I \}.$$

We incorporate boundary condition g_N in the space, by imposing the degrees of freedom associated with the edges on the Neumann part of the boundary Γ_N . We set the discrete trial and test spaces for the fluxes space as

$$\begin{aligned} \boldsymbol{\Sigma}_{n, g_N} &:= \{ \boldsymbol{\tau}_n \in \boldsymbol{\Sigma}_n \mid \mathbf{n} \cdot \boldsymbol{\tau}_n = g_N \text{ on } e \text{ if } e \subset \Gamma_N \}, \\ \boldsymbol{\Sigma}_{n, 0} &:= \{ \boldsymbol{\tau}_n \in \boldsymbol{\Sigma}_n \mid \mathbf{n} \cdot \boldsymbol{\tau}_n = 0 \text{ on } e \text{ if } e \subset \Gamma_N \}. \end{aligned}$$

With each global space, we associate a set of unisolvent degrees of freedom, obtained by a standard $H(\operatorname{div})$ -conforming Raviart-Thomas coupling.

Remark 4. Although the functions in $\boldsymbol{\Sigma}_n(K)$ are not available in closed form inside the elements, their divergence is computable from degrees of freedom (15) and (16) *explicitly*. Thence, we are able to compute exactly bilinear form $b(\boldsymbol{\tau}_n, v_n)$ (7) for all $\boldsymbol{\tau}_n \in \boldsymbol{\Sigma}_n$ and $v_n \in V_n$. \blacksquare

Projector. We introduce the $L^2(K)$ vector projector $\boldsymbol{\Pi}_p^0 : \boldsymbol{\Sigma}_n(K) \rightarrow \mathcal{G}_p(K)$ into the gradient of polynomials on each element $K \in \mathcal{T}_n$:

$$a^K(\boldsymbol{\tau}_n - \boldsymbol{\Pi}_p^0 \boldsymbol{\tau}_n, \mathbf{q}_p) = 0 \quad \forall \boldsymbol{\tau}_n \in \boldsymbol{\Sigma}_n(K), \ \forall \mathbf{q}_p \in \mathcal{G}_p(K). \quad (18)$$

This projector is computable from the degrees of freedom in (15)–(17). To see this, we observe that

$$a^K(\boldsymbol{\tau}_n, \nabla q_{p+1}) = -a^K(\operatorname{div}(\boldsymbol{\tau}_n), q_{p+1}) + (\boldsymbol{\tau}_n \cdot \mathbf{n}, q_{p+1})_{0, \partial K} \quad \forall \boldsymbol{\tau}_n \in \boldsymbol{\Sigma}_n(K), \ \forall q_{p+1} \in \mathbb{P}_{p+1}(K).$$

The term on the right-hand side is computable using an integration by parts and degrees of freedom (15) and (16). Interestingly enough, projector $\boldsymbol{\Pi}_p^0$ can be generalized to a projector into spaces of gradients of polynomials with arbitrary degree, i.e., $[\mathbb{P}_{\tilde{p}}(K)]^2$ for all $\tilde{p} \in \mathbb{N}$. Indeed, both the divergence and the normal components of functions in virtual element spaces are known explicitly.

Discrete bilinear forms and right-hand side. As for bilinear form $a(\cdot, \cdot)$, we proceed similarly to what is done for the primal formulation in Section 2.2. First, consider the splitting

$$a(\boldsymbol{\sigma}, \boldsymbol{\tau}) = \sum_{K \in \mathcal{T}_n} \int_K \mathbb{K}^{-1} \boldsymbol{\sigma} \cdot \boldsymbol{\tau} =: \sum_{K \in \mathcal{T}_n} a^K(\boldsymbol{\sigma}|_K, \boldsymbol{\tau}|_K) \quad \forall \boldsymbol{\sigma}, \boldsymbol{\tau} \in \boldsymbol{\Sigma}.$$

Projector $\boldsymbol{\Pi}_p^0$ in (18) allows us to construct a computable discrete bilinear form mimicking $a(\cdot, \cdot)$. For all $K \in \mathcal{T}_n$, consider any bilinear form $S^K : \ker(\boldsymbol{\Pi}_p^0) \times \ker(\boldsymbol{\Pi}_p^0) \rightarrow \mathbb{R}$, computable via the degrees of freedom and satisfying

$$\alpha_* a^K(\boldsymbol{\tau}_n, \boldsymbol{\tau}_n) \leq S^K(\boldsymbol{\tau}_n, \boldsymbol{\tau}_n) \leq \alpha^* a^K(\boldsymbol{\tau}_n, \boldsymbol{\tau}_n). \quad (19)$$

The constants $0 < \alpha_* \leq \alpha^* < +\infty$ depend possibly on the geometry of the polygonal decomposition, on degree of accuracy p , and on \mathbb{K} , but must be independent of size h_K of element K .

Introducing local discrete bilinear forms

$$a_n^K(\boldsymbol{\sigma}_n, \boldsymbol{\tau}_n) := a^K(\boldsymbol{\Pi}_p^0 \boldsymbol{\sigma}_n, \boldsymbol{\Pi}_p^0 \boldsymbol{\tau}_n) + S^K((\mathbf{I} - \boldsymbol{\Pi}_p^0) \boldsymbol{\sigma}_n, (\mathbf{I} - \boldsymbol{\Pi}_p^0) \boldsymbol{\tau}_n) \quad \forall \boldsymbol{\sigma}_n, \boldsymbol{\tau}_n \in \boldsymbol{\Sigma}_n(K),$$

we define global discrete bilinear form

$$a_n(\boldsymbol{\sigma}_n, \boldsymbol{\tau}_n) := \sum_{K \in \mathcal{T}_n} a_n^K(\boldsymbol{\sigma}_n|_K, \boldsymbol{\tau}_n|_K) \quad \forall \boldsymbol{\sigma}_n, \boldsymbol{\tau}_n \in \boldsymbol{\Sigma}_n.$$

Following [21], global discrete bilinear form $a_n(\cdot, \cdot)$ is coercive with constant $\min(k_*^{*-1}, \min_{K \in \mathcal{T}_n} \alpha_*)$ and continuous with constant $\max(k_*^{-1}, \max_{K \in \mathcal{T}_n} \alpha^*)$ on the discrete kernel

$$\mathcal{K}_n = \{\boldsymbol{\tau}_n \in \boldsymbol{\Sigma}_n \mid b(\boldsymbol{\tau}_n, v_n) = 0 \text{ for all } v_n \in V_n\}. \quad (20)$$

Discrete kernel \mathcal{K}_n is contained in continuous kernel \mathcal{K} , which is defined as

$$\mathcal{K} := \{\boldsymbol{\tau} \in \boldsymbol{\Sigma} \mid b(\boldsymbol{\tau}, v) = 0 \text{ for all } v \in V\}.$$

As far as the right-hand side $(f, v_n)_{0, \Omega}$ is concerned, we recall that v_n is a piecewise polynomial. Hence, the right-hand side is computable assuming to be able to integrate $L^1(K)$ functions exactly.

The virtual element method for the mixed formulation. The virtual element method tailored for the approximation of the problem in mixed form (8) reads

$$\begin{cases} \text{find } (\boldsymbol{\sigma}_n, u_n) \in \boldsymbol{\Sigma}_{n, g_N} \times V_n \text{ such that} \\ a_n(\boldsymbol{\sigma}_n, \boldsymbol{\tau}_n) + b(\boldsymbol{\tau}_n, u_n) = -(g_D, \mathbf{n} \cdot \boldsymbol{\tau}_n)_{0, \Gamma_D} \quad \forall \boldsymbol{\tau}_n \in \boldsymbol{\Sigma}_{n, 0} \\ b(\boldsymbol{\sigma}_n, v_n) = (-f, v_n)_{0, \Omega} \quad \forall v_n \in V_n. \end{cases} \quad (21)$$

The definition of the trial and test spaces, and the second equation in (21) entail that

$$\operatorname{div}(\boldsymbol{\sigma}_n) = \Pi_{p-1}^0 f \quad \text{in } \Omega. \quad (22)$$

Remark 5. So far, we have discussed the construction of virtual elements with uniform degree of accuracy over all the elements. As already highlighted in Remark 3, the flexibility of the virtual element framework allows for the construction of global spaces with variable degrees of accuracy. Since the construction of spaces with variable degree of accuracy follows along the same lines as of the primal formulation case, we omit the details of the construction. ■

2.4 Providing explicit stabilizations

Here, we address the issue of providing computable stabilizations with bounds on constants $\tilde{\alpha}_*$, $\tilde{\alpha}^*$, α_* , and α^* that are explicit in terms of degree of accuracy p ; see (12) and (19), respectively. We pose ourselves in the situation of uniform degree of accuracy over all the elements. The variable case can be tackled as in [8]; see also Remarks 3 and 5 for further comments on this aspect.

Theoretical stabilizations. A stabilization for the primal formulation with explicit bounds on stabilization constants $\tilde{\alpha}_*$ and $\tilde{\alpha}^*$ can be found in [8, Section 4]. Assuming that $\mathbb{K} = 1$, such stabilization reads

$$\tilde{S}^K(\tilde{u}_n, \tilde{v}_n) = \frac{h_K^2}{p^2} (\tilde{\Pi}_{p-2}^0 \tilde{u}_n, \tilde{\Pi}_{p-2}^0 \tilde{v}_n)_{0, K} + \frac{h_K}{p} (\tilde{u}_n, \tilde{v}_n)_{0, \partial K}. \quad (23)$$

The following bounds were proven in [8, Theorem 2]:

$$\tilde{\alpha}_*(p) \gtrsim p^{-5}, \quad \tilde{\alpha}^*(p) \lesssim p^2.$$

Such bounds are extremely crude. As numerically investigated in [8, Section 4.1], the actual dependence on p is much milder.

It is possible to modify stabilization (23) to the instance of variable \mathbb{K} :

$$\tilde{S}^K(\tilde{u}_n, \tilde{v}_n) = \frac{h_K^2}{p^2} (\mathbb{K} \tilde{\Pi}_{p-2}^0 \tilde{u}_n, \tilde{\Pi}_{p-2}^0 \tilde{v}_n)_{0, K} + \frac{h_K}{p} (\mathbb{K} \tilde{u}_n, \tilde{v}_n)_{0, \partial K}.$$

Exploiting the assumptions on \mathbb{K} in (3), the bounds on the stability constants become

$$\tilde{\alpha}_*(p) \gtrsim k_* p^{-5}, \quad \tilde{\alpha}^*(p) \lesssim k^* p^2. \quad (24)$$

Next, we focus on an explicit choice for stabilization S^K (19) in the mixed VEM (21). To the best of our knowledge, no stabilization for the mixed version of VEM has been constructed explicitly so far. Rather, stabilizations with a reasonable scaling were suggested. Hence, in the following, we are presenting a novel explicit construction of such a stabilization.

For all $K \in \mathcal{T}_n$ and for all $\boldsymbol{\sigma}_n$ and $\boldsymbol{\tau}_n$ in the kernel of the L^2 projector used in [21], we define the stabilization

$$\begin{aligned} S^K(\boldsymbol{\sigma}_n, \boldsymbol{\tau}_n) &= h_K(\mathbb{K}^{-1} \mathbf{n} \cdot \boldsymbol{\sigma}_n, \mathbf{n} \cdot \boldsymbol{\tau}_n)_{0, \partial K} \\ &\quad + h_K^2(\mathbb{K}^{-1} \operatorname{div} \boldsymbol{\sigma}_n, \operatorname{div} \boldsymbol{\tau}_n)_{0, K} + h_K^2(\mathbb{K}^{-1} \operatorname{rot} \boldsymbol{\sigma}_n, \operatorname{rot} \boldsymbol{\tau}_n)_{0, K}. \end{aligned} \quad (25)$$

Thanks to the choice of degrees of freedom (15)–(17), stabilization S^K is computable explicitly. Recall the following four lemmata from [8, 14, 38, 42], which will be instrumental in the analysis of stabilization (25).

Lemma 2.3. *For all convex Lipschitz domains $K \subset \mathbb{R}^2$ with diameter 1 and all $\boldsymbol{\tau} \in H(\operatorname{div}, K) \cap H(\operatorname{rot}, K)$ with $\mathbf{n} \cdot \boldsymbol{\tau} = 0$, the following bound is valid:*

$$\|\boldsymbol{\tau}\|_{0, K} \lesssim (\|\operatorname{div}(\boldsymbol{\tau})\|_{0, K} + \|\operatorname{rot}(\boldsymbol{\tau})\|_{0, K}).$$

Proof. See [38, Theorem 4.4]. □

Lemma 2.4. *For all simply connected and bounded Lipschitz domains $K \subset \mathbb{R}^2$ with diameter 1 and for all $\boldsymbol{\tau} \in H(\operatorname{div}, K) \cap H(\operatorname{rot}, K)$ with $\operatorname{div}(\boldsymbol{\tau}) = 0$ and $\mathbf{n} \cdot \boldsymbol{\tau} \in L^2(\Omega)$, the following bound is valid:*

$$\|\boldsymbol{\tau}\|_{0, K} \lesssim (\|\operatorname{rot}(\boldsymbol{\tau})\|_{0, K} + \|\mathbf{n} \cdot \boldsymbol{\tau}\|_{0, \partial K}).$$

Proof. This is the two dimensional counterpart of [42, Corollary 3.51]. □

Lemma 2.5. *Let K be a polygon with diameter 1. Assume that its edges have a length ≈ 1 . Let b_e be the piecewise quadratic bubble function on ∂K annihilating at the vertices of K . Then, for all piecewise polynomials q_p over ∂K , the following polynomial inverse inequality is valid:*

$$\|q_p\|_{0, \partial K} \lesssim p \|q_p b_e^{\frac{1}{2}}\|_{0, \partial K}. \quad (26)$$

Proof. See [14, Lemma 4]. □

Lemma 2.6. *Let K be a polygon with diameter 1. Assume that its edges have a length ≈ 1 . Then, for all $q_p \in \mathbb{P}_p(K)$, the following polynomial inverse inequality is valid:*

$$\|q_p\|_{0, K} \lesssim p^2 \|q_p\|_{-1, K} := p^2 \sup_{\Phi \in H_0^1(K)} \frac{(q_p, \Phi)_{0, K}}{|\Phi|_{1, K}}. \quad (27)$$

Proof. See [8, Theorem 5]. □

We prove the following result.

Proposition 2.7. *For all convex $K \in \mathcal{T}_n$, bilinear form $S^K(\cdot, \cdot)$ (25) is such that the following bounds on constants α_* and α^* in (19) are valid:*

$$\alpha_* \gtrsim (k^*)^{-1}, \quad \alpha^* \lesssim (k_*)^{-1} p^6. \quad (28)$$

Proof. Throughout the proof, we assume that $h_K = 1$. The general case follows from a scaling argument. Besides, it suffices to prove the statement for $\mathbb{K} = 1$. The general case follows from assumptions (3) on \mathbb{K} .

First, we show the bound on α_* . Given $\boldsymbol{\tau}_n \in \boldsymbol{\Sigma}_n(K)$, we define functions $\tilde{\boldsymbol{\tau}}_n$ and $\boldsymbol{\tau}_n^{\partial K}$ as

$$\mathbf{n}|_{\partial K} \cdot \tilde{\boldsymbol{\tau}}_n = 0, \quad \operatorname{div}(\tilde{\boldsymbol{\tau}}_n) = \operatorname{div}(\boldsymbol{\tau}_n), \quad \operatorname{rot}(\tilde{\boldsymbol{\tau}}_n) = \operatorname{rot}(\boldsymbol{\tau}_n) \quad (29)$$

and

$$\mathbf{n}|_{\partial K} \cdot \boldsymbol{\tau}_n^{\partial K} = \mathbf{n}|_{\partial K} \cdot \boldsymbol{\tau}_n, \quad \operatorname{div}(\boldsymbol{\tau}_n^{\partial K}) = 0, \quad \operatorname{rot}(\boldsymbol{\tau}_n^{\partial K}) = 0. \quad (30)$$

Clearly, $\boldsymbol{\tau}_n = \tilde{\boldsymbol{\tau}}_n + \boldsymbol{\tau}_n^{\partial K}$. Using Lemmata 2.3 and 2.4 we deduce

$$\begin{aligned} \|\boldsymbol{\tau}_n\|_{0,K} &\leq \|\tilde{\boldsymbol{\tau}}_n\|_{0,K} + \|\boldsymbol{\tau}_n^{\partial K}\|_{0,K} \\ &\lesssim \|\operatorname{rot}(\boldsymbol{\tau}_n^{\partial K})\|_{0,K} + \|\mathbf{n} \cdot \boldsymbol{\tau}_n^{\partial K}\|_{0,\partial K} + \|\operatorname{rot}(\tilde{\boldsymbol{\tau}}_n)\|_{0,K} + \|\operatorname{div}(\tilde{\boldsymbol{\tau}}_n)\|_{0,K}. \end{aligned}$$

Identities (29) and (30) imply

$$\|\boldsymbol{\tau}_n\|_{0,K} \lesssim \|\mathbf{n} \cdot \boldsymbol{\tau}_n\|_{0,\partial K} + \|\operatorname{div}(\boldsymbol{\tau}_n)\|_{0,K},$$

which is the desired bound.

Next, we deal with the bound on α^* . It suffices to show a bound for the terms on the right-hand side of (25) by some constant depending on p times $\|\boldsymbol{\tau}_n\|_{0,K}$. Since $\mathbf{n} \cdot \boldsymbol{\tau}$ is a piecewise polynomial on ∂K , the following polynomial inverse inequality is valid:

$$\|\mathbf{n} \cdot \boldsymbol{\tau}_n\|_{0,\partial K} \lesssim p \|\mathbf{n} \cdot \boldsymbol{\tau}_n\|_{-\frac{1}{2},\partial K}. \quad (31)$$

In order to prove (31), introduce b_e the piecewise quadratic bubble function on ∂K annihilating at the vertices of K . Use Lemma 2.5 and definition (1) to get, for a piecewise polynomial q_p over ∂K ,

$$\|q_p\|_{0,\partial K} \stackrel{(26)}{\lesssim} p \frac{(q_p, q_p b_e)_{0,K}}{\|q_p b_e^{\frac{1}{2}}\|_{0,\partial K}} \leq p \frac{(q_p, q_p b_e)_{0,K}}{\|q_p b_e\|_{0,\partial K}} \leq p \sup_{w \in H^{\frac{1}{2}}(\partial K)} \frac{(q_p, w)_{0,\partial K}}{\|w\|_{0,\partial K}} =: p \|q_p\|_{-\frac{1}{2},\partial K}.$$

Finally, substituting q_p with $\mathbf{n} \cdot \boldsymbol{\tau}_n$, we get (31).

Using (31) and inequality [42, Theorem 3.24], we obtain

$$\|\mathbf{n} \cdot \boldsymbol{\tau}_n\|_{0,\partial K} \lesssim p (\|\boldsymbol{\tau}_n\|_{0,K} + \|\operatorname{div}(\boldsymbol{\tau}_n)\|_{0,K}).$$

We show an upper bound on the divergence term, i.e., the second term appearing on the right-hand side of (25). Use Lemma 2.6 substituting q_p with $\operatorname{div}(\boldsymbol{\tau}_n)$ in (27), and an integration by parts, to get

$$\begin{aligned} \|\operatorname{div}(\boldsymbol{\tau}_n)\|_{0,K} &\lesssim p^2 \|\operatorname{div}(\boldsymbol{\tau}_n)\|_{-1,K} := p^2 \sup_{\Phi \in H_0^1(K)} \frac{(\operatorname{div}(\boldsymbol{\tau}_n), \Phi)_{0,K}}{|\Phi|_{1,K}} \\ &= p^2 \sup_{\Phi \in H_0^1(K)} \frac{(\boldsymbol{\tau}_n, \nabla \Phi)_{0,K}}{|\Phi|_{1,K}} \leq p^2 \|\boldsymbol{\tau}_n\|_{0,K}. \end{aligned}$$

This concludes the proof of the upper bound on the first two terms on the right-hand side of (25).

Finally, we use Lemma 2.6 substituting q_p with $\operatorname{rot}(\boldsymbol{\tau}_n)$ to show the upper bound on the third term on the right-hand side of (25). Denoting the vectorial rotor by \mathbf{curl} , we can write

$$\begin{aligned} \|\operatorname{rot}(\boldsymbol{\tau}_n)\|_{0,K} &\lesssim p^2 \|\operatorname{rot}(\boldsymbol{\tau}_n)\|_{-1,K} := p^2 \sup_{\Phi \in H_0^1(K)} \frac{(\operatorname{rot}(\boldsymbol{\tau}_n), \Phi)_{0,K}}{|\Phi|_{1,K}} \\ &= p^2 \sup_{\Phi \in H_0^1(K)} \frac{(\boldsymbol{\tau}_n, \mathbf{curl} \Phi)_{0,K}}{|\Phi|_{1,K}} \lesssim p^2 \|\boldsymbol{\tau}_n\|_{0,K}, \end{aligned}$$

whence the assertion follows. \square

Note that the assumption on the convexity of the elements in Proposition 2.7 is needed only to apply Lemma 2.3.

Remark 6. As for the h -version of the method, stabilization S^K (25) can be employed as well. \blacksquare

Practical stabilizations. In the numerical experiments of Sections 4 and 6, we will not employ stabilizations (23) and (25). Rather, we suggest to use variants of the so-called D-recipe stabilization; see [9]. In fact, as analyzed in [31, 39], the D-recipe leads to an extremely robust performance of the method (13), and is straightforward to implement.

We employ the following stabilization for the primal formulation: given $N^{\tilde{V}_n} := \dim(\tilde{V}_n(K))$, for all $K \in \mathcal{T}_n$, given $\{\tilde{\varphi}_j\}_{j=1}^{N^{\tilde{V}_n}}$ the canonical basis of local space $\tilde{V}_n(K)$,

$$\tilde{S}^K(\tilde{\varphi}_j, \tilde{\varphi}_\ell) = \max \left(|\mathbb{K}|, (\mathbb{K} \nabla \tilde{\Pi}_p^\nabla \tilde{\varphi}_j, \nabla \tilde{\Pi}_p^\nabla \tilde{\varphi}_\ell)_{0,K} \right) \delta_{j,\ell} \quad \forall j, \ell = 1, \dots, N^{\tilde{V}_n}. \quad (32)$$

Here, $\delta_{j,\ell}$ denotes the Kronecker delta, whereas projector $\tilde{\Pi}_p^\nabla$ is defined in (11).

As for the D-recipe stabilization for the mixed formulation, we employ the following: given $N^{\Sigma_n} := \dim(\Sigma_n(K))$, for all $K \in \mathcal{T}_n$, given $\{\varphi_j\}_{j=1}^{N^{\Sigma_n}}$ the canonical basis of local space $\Sigma_n(K)$,

$$S^K(\varphi_j, \varphi_\ell) = \max \left(|\mathbb{K}^{-1}| h_K^2, (\mathbb{K}^{-1} \mathbf{\Pi}_p^0 \varphi_j, \mathbf{\Pi}_p^0 \varphi_\ell)_{0,K} \right) \delta_{j,\ell} \quad \forall j, \ell = 1, \dots, N^{\Sigma_n}. \quad (33)$$

Projector $\mathbf{\Pi}_p^0$ is defined in (18).

As already mentioned, in Section 4 below, we show the numerical experiments for the adaptive method employing the practical stabilizations. However, we present some numerics comparing the practical and theoretical stabilizations for the p -version a priori mixed VEM. Moreover, we numerically demonstrate that the convexity assumption in Proposition 2.7 is only a theoretical artefact with no effect whatsoever on the practical behaviour of the method.

2.5 Well-posedness of the two virtual element methods

In this section, we prove the well-posedness of the primal and mixed VEM in (13) and (21).

The well-posedness of primal VEM formulation (13) follows from the continuity and coercivity of discrete bilinear form $\tilde{a}_n(\cdot, \cdot)$, the continuity of the discrete right-hand side, and Lax-Milgram lemma.

As for mixed VEM formulation (21), we need two ingredients in order to prove the well-posedness of the method. The first one is the continuity and the coercivity of bilinear form $a_n(\cdot, \cdot)$ on discrete kernel (20). The second one is the validity of the inf-sup condition for bilinear form $b(\cdot, \cdot)$, with explicit bounds on the inf-sup constant in terms of h and p . The remainder of the section is devoted to prove such an inf-sup condition.

Theorem 2.8. *There exists a constant $\beta_n > 0$ independent of the discretization parameters, such that for all $v_n \in V_n$ there exists $\boldsymbol{\tau}_n \in \Sigma_{n,0}$ satisfying*

$$b(v_n, \boldsymbol{\tau}_n) \geq \beta_n \|\boldsymbol{\tau}_n\|_{\text{div}, \Omega} \|v_n\|_{0, \Omega}. \quad (34)$$

Constant β_n is known in closed form:

$$\beta_n = \left(c_\Omega \frac{|\Omega|^{\frac{1}{2}}}{|\Gamma_D|^{\frac{1}{2}}} + c_\Omega + 1 \right)^{-1},$$

where c_Ω is a constant depending only on the shape of Ω , which will be detailed in the proof.

Proof. To each $v_n \in V_n$, we associate a function $\boldsymbol{\tau}_n \in \Sigma_{n,0}$ as follows. For all internal edges $e \in \mathcal{E}_n^I$, we fix $\mathbf{n} \cdot \boldsymbol{\tau}_n = 0$ on e . We impose this constraint, in order to fix a function $\boldsymbol{\tau}_n$ in virtual element space $\Sigma_{n,0}$. We define $\boldsymbol{\tau}_n$ as the solution to the global div-rot problem

$$\begin{cases} \text{div}(\boldsymbol{\tau}_n) = v_n & \text{in } \Omega \\ \text{rot}(\boldsymbol{\tau}_n) = 0 & \text{in } \Omega \\ \mathbf{n} \cdot \boldsymbol{\tau}_n = c_\tau & \text{on } \Gamma_D \\ \mathbf{n} \cdot \boldsymbol{\tau}_n = 0 & \text{on } \Gamma_N. \end{cases} \quad (35)$$

Constant c_τ has to be chosen, so that the compatibility condition of problem (35) is fulfilled. In other words, the following must be true:

$$|\Gamma_D|c_\tau = \int_{\Gamma_D} c_\tau = \int_{\Gamma_D} \mathbf{n} \cdot \boldsymbol{\tau}_n = \int_{\partial\Omega} \mathbf{n} \cdot \boldsymbol{\tau}_n = \int_{\Omega} \operatorname{div}(\boldsymbol{\tau}_n) = \int_{\Omega} v_n.$$

This is equivalent to ask

$$c_\tau = \frac{1}{|\Gamma_D|} \int_{\Omega} v_n. \quad (36)$$

With this choice, problem (35) is well-posed, whence it follows that $\boldsymbol{\tau}_n$ is well-defined; see, e.g., [3] and the references therein.

Applying [30, Remark p. 367] and Friedrichs' inequality [42, Corollary 3.51] yields

$$\|\boldsymbol{\tau}_n\|_{0,\Omega} \leq c_\Omega (\|\mathbf{n} \cdot \boldsymbol{\tau}_n\|_{0,\partial\Omega} + \|\operatorname{div}(\boldsymbol{\tau}_n)\|_{0,\Omega}),$$

where c_Ω is a positive constant depending on Ω solely.

We deduce

$$\begin{aligned} \|\boldsymbol{\tau}_n\|_{0,\Omega} &\leq c_\Omega (\|\mathbf{n} \cdot \boldsymbol{\tau}_n\|_{0,\Gamma_D} + \|\operatorname{div}(\boldsymbol{\tau}_n)\|_{0,\Omega}) \stackrel{(35)}{=} c_\Omega \left(|\Gamma_D|^{\frac{1}{2}} |c_\tau| + \|\operatorname{div}(\boldsymbol{\tau}_n)\|_{0,\Omega} \right) \\ &\stackrel{(36)}{=} c_\Omega \left(\frac{1}{|\Gamma_D|^{\frac{1}{2}}} \left| \int_{\Omega} v_n \right| + \|\operatorname{div}(\boldsymbol{\tau}_n)\|_{0,\Omega} \right) \\ &\stackrel{(35)}{=} c_\Omega \left(\frac{1}{|\Gamma_D|^{\frac{1}{2}}} \left| \int_{\Omega} \operatorname{div}(\boldsymbol{\tau}_n) \right| + \|\operatorname{div}(\boldsymbol{\tau}_n)\|_{0,\Omega} \right) \leq c_\Omega \left(\frac{|\Omega|^{\frac{1}{2}}}{|\Gamma_D|^{\frac{1}{2}}} + 1 \right) \|\operatorname{div}(\boldsymbol{\tau}_n)\|_{0,\Omega}. \end{aligned}$$

This implies

$$\|\boldsymbol{\tau}_n\|_{\operatorname{div},\Omega} \leq \left(c_\Omega \frac{|\Omega|^{\frac{1}{2}}}{|\Gamma_D|^{\frac{1}{2}}} + c_\Omega + 1 \right) \|\operatorname{div}(\boldsymbol{\tau}_n)\|_{0,\Omega} = \beta_n^{-1} \|\operatorname{div}(\boldsymbol{\tau}_n)\|_{0,\Omega}. \quad (37)$$

Note that

$$\|v_n\|_{0,\Omega} = \frac{(v_n, v_n)_{0,\Omega}}{\|v_n\|_{0,\Omega}} \stackrel{(35)}{=} \frac{(v_n, \operatorname{div}(\boldsymbol{\tau}_n))_{0,\Omega}}{\|\operatorname{div}(\boldsymbol{\tau}_n)\|_{0,\Omega}}.$$

Apply (37) to this identity, and deduce the inf-sup condition

$$\|v_n\|_{0,\Omega} \leq \frac{1}{\beta_n} \frac{(v_n, \operatorname{div}(\boldsymbol{\tau}_n))_{0,\Omega}}{\|\boldsymbol{\tau}_n\|_{\operatorname{div},\Omega}}.$$

□

Discrete inf-sup condition (34), together with the definition of the continuity of the discrete bilinear forms $a_n(\cdot, \cdot)$ and $b(\cdot, \cdot)$, and the coercivity of $a_n(\cdot, \cdot)$ on discrete kernel \mathcal{K}_n (20), is sufficient to prove the well-posedness of method (21); see [17]. In fact, a lifting argument allows us to seek solutions in discrete space $\boldsymbol{\Sigma}_{n,0}$, i.e., solutions with zero normal trace on Γ_N .

Remark 7. We have proved Theorem 2.8 assuming that $\Gamma_D \neq \emptyset$, which is an assumption stipulated in Section 1. The case of pure Neumann boundary conditions has to be dealt with slightly differently. The primal virtual element space has to be endowed with a zero average constraint. In order to prove the inf-sup condition one should proceed as in [21, Theorem 4.2 and Corollary 4.3]. Besides, one ought to prove that the best approximant in mixed virtual element spaces converges optimally in terms of h and p to a target function, so that the inf-sup constant is p -robust. This can be indeed proven by defining the best approximation in virtual element spaces as the degrees of freedom interpolant of the continuous function to approximate. However, whatever boundary conditions we pick, the inf-sup constant is p -robust. To the best of our knowledge, this is not the case in the discontinuous Galerkin setting for mixed problems; see, e.g., [47, Section 4.2]. ■

3 The hypercircle method for the VEM

The aim of the present section is to construct an equilibrated a posteriori error estimator and to prove lower and upper bounds of such error estimator in terms of the exact error. In Section 3.1, we show an identity, which is the basic tile of the a posteriori error analysis and exhibit the equilibrated error estimator. Next, in Sections 3.2 and 3.3, we show its reliability and efficiency.

3.1 The equilibrated a posteriori error estimator

Given \tilde{u} , $\boldsymbol{\sigma}$, \tilde{u}_n , and $\boldsymbol{\sigma}_n$ the solutions to (6), (8), (13), and (21), respectively, we observe that

$$\|\mathbb{K}^{\frac{1}{2}}(\nabla\tilde{u}-\nabla\tilde{u}_n)\|_{0,\Omega}^2+\|\mathbb{K}^{-\frac{1}{2}}(\boldsymbol{\sigma}-\boldsymbol{\sigma}_n)\|_{0,\Omega}^2=\|\mathbb{K}^{\frac{1}{2}}\nabla\tilde{u}_n+\mathbb{K}^{-\frac{1}{2}}\boldsymbol{\sigma}_n\|_{0,\Omega}^2-2\int_{\Omega}\nabla(\tilde{u}-\tilde{u}_n)\cdot(\boldsymbol{\sigma}-\boldsymbol{\sigma}_n). \quad (38)$$

In order to show this identity, we observe that (9) entails

$$\begin{aligned} & \|\mathbb{K}^{\frac{1}{2}}\nabla\tilde{u}_n+\mathbb{K}^{-\frac{1}{2}}\boldsymbol{\sigma}_n\|_{0,\Omega}^2-2\int_{\Omega}\nabla(\tilde{u}-\tilde{u}_n)\cdot(\boldsymbol{\sigma}-\boldsymbol{\sigma}_n) \\ &= \int_{\Omega}\mathbb{K}^{\frac{1}{2}}(\nabla\tilde{u}_n-\nabla\tilde{u})\cdot\left(\mathbb{K}^{\frac{1}{2}}\nabla\tilde{u}_n+\mathbb{K}^{-\frac{1}{2}}\boldsymbol{\sigma}_n\right)+\int_{\Omega}\left(\mathbb{K}^{-\frac{1}{2}}\boldsymbol{\sigma}_n+\mathbb{K}^{\frac{1}{2}}\nabla\tilde{u}\right)\cdot\left(\mathbb{K}^{\frac{1}{2}}\nabla\tilde{u}_n+\mathbb{K}^{-\frac{1}{2}}\boldsymbol{\sigma}_n\right) \\ & \quad -2\int_{\Omega}\mathbb{K}^{\frac{1}{2}}\nabla(\tilde{u}-\tilde{u}_n)\cdot\mathbb{K}^{-\frac{1}{2}}(\boldsymbol{\sigma}-\boldsymbol{\sigma}_n) \\ &= \int_{\Omega}\mathbb{K}^{\frac{1}{2}}(\nabla\tilde{u}-\nabla\tilde{u}_n)\cdot\left(-\mathbb{K}^{\frac{1}{2}}\nabla\tilde{u}_n-\mathbb{K}^{-\frac{1}{2}}\boldsymbol{\sigma}_n+\mathbb{K}^{\frac{1}{2}}\nabla\tilde{u}+\mathbb{K}^{-\frac{1}{2}}\boldsymbol{\sigma}_n\right) \\ & \quad +\int_{\Omega}\mathbb{K}^{-\frac{1}{2}}(\boldsymbol{\sigma}-\boldsymbol{\sigma}_n)\cdot\left(-\mathbb{K}^{\frac{1}{2}}\nabla\tilde{u}_n-\mathbb{K}^{-\frac{1}{2}}\boldsymbol{\sigma}_n+\mathbb{K}^{-\frac{1}{2}}\boldsymbol{\sigma}+\mathbb{K}^{\frac{1}{2}}\nabla\tilde{u}_n\right) \\ &= \int_{\Omega}\mathbb{K}(\nabla\tilde{u}-\nabla\tilde{u}_n)\cdot(\nabla\tilde{u}-\nabla u_n)+\int_{\Omega}\mathbb{K}^{-1}(\boldsymbol{\sigma}-\boldsymbol{\sigma}_n)\cdot(\boldsymbol{\sigma}-\boldsymbol{\sigma}_n), \end{aligned}$$

which is (38).

We rewrite the last term on the right-hand side of (38) using an integration by parts element by element: for all $K \in \mathcal{T}_n$,

$$-\int_K\nabla(\tilde{u}-\tilde{u}_n)\cdot(\boldsymbol{\sigma}-\boldsymbol{\sigma}_n)=\int_K(\tilde{u}-\tilde{u}_n)\operatorname{div}(\boldsymbol{\sigma}-\boldsymbol{\sigma}_n)-\int_{\partial K}(\tilde{u}-\tilde{u}_n)\mathbf{n}\cdot(\boldsymbol{\sigma}-\boldsymbol{\sigma}_n).$$

We reshape the first term on the right-hand side. Recalling that $\operatorname{div}(\boldsymbol{\sigma})=f$ and $\operatorname{div}(\boldsymbol{\sigma}_n)=\Pi_{p-1}^0f$, see (22), we write

$$\int_K(\tilde{u}-\tilde{u}_n)(\operatorname{div}(\boldsymbol{\sigma})-\operatorname{div}(\boldsymbol{\sigma}_n))=\int_K(u-\tilde{u}_n)(f-\Pi_{p-1}^0f).$$

We collect all the contributions and deduce that, for every piecewise discontinuous polynomial q_{p-1} of degree $p-1$ over \mathcal{T}_n ,

$$\begin{aligned} & \|\mathbb{K}^{\frac{1}{2}}\nabla(\tilde{u}-\tilde{u}_n)\|_{0,\Omega}^2+\|\mathbb{K}^{-\frac{1}{2}}(\boldsymbol{\sigma}-\boldsymbol{\sigma}_n)\|_{0,\Omega}^2 \\ &= \|\mathbb{K}^{\frac{1}{2}}\nabla\tilde{u}_n+\mathbb{K}^{-\frac{1}{2}}\boldsymbol{\sigma}_n\|_{0,\Omega}^2+2\int_{\Omega}(\tilde{u}-\tilde{u}_n-q_{p-1})(f-\Pi_{p-1}^0f) \\ & \quad -2\sum_{K\in\mathcal{T}_n}\int_{\partial K}(\tilde{u}-\tilde{u}_n)\mathbf{n}\cdot(\boldsymbol{\sigma}-\boldsymbol{\sigma}_n). \end{aligned} \quad (39)$$

The internal interface contributions appearing in the last term on the right-hand side of (39) are zero. The virtual element spaces have been tailored so that this property is fulfilled. Furthermore, the boundary contributions disappear thanks to assumption **(D)**.

Thus, we write

$$\begin{aligned} & \|\mathbb{K}^{\frac{1}{2}}\nabla(\tilde{u}-\tilde{u}_n)\|_{0,\Omega}^2+\|\mathbb{K}^{-\frac{1}{2}}(\boldsymbol{\sigma}-\boldsymbol{\sigma}_n)\|_{0,\Omega}^2 \\ &= \|\mathbb{K}^{\frac{1}{2}}\nabla\tilde{u}_n+\mathbb{K}^{-\frac{1}{2}}\boldsymbol{\sigma}_n\|_{0,\Omega}^2+2\int_{\Omega}(\tilde{u}-\tilde{u}_n-q_{p-1})(f-\Pi_{p-1}^0f). \end{aligned} \quad (40)$$

In the two forthcoming Sections 3.2 and 3.3, we show upper and lower bounds on the right-hand side of (40). This will give rise to a natural choice for the equilibrated error estimator. Henceforth, we refer to the square root of the left-hand side of (40) as to the exact error of the method. In particular, the exact error is the square root of the sum of the square of the error of primal (13) and mixed (21) VEMs.

The error estimator. Since $\|\mathbb{K}^{\frac{1}{2}}\nabla\tilde{u}_n + \mathbb{K}^{-\frac{1}{2}}\boldsymbol{\sigma}_n\|_{0,\Omega}$ is not computable, we propose the following local equilibrated error estimators

$$\begin{aligned} \eta_{\text{eq},K}^2 &:= \|\mathbb{K}^{\frac{1}{2}}\nabla\tilde{\Pi}_p^\nabla\tilde{u}_n + \mathbb{K}^{-\frac{1}{2}}\mathbf{\Pi}_p^0\boldsymbol{\sigma}_n\|_{0,K}^2 \\ &\quad + \left[\tilde{S}^K((I - \tilde{\Pi}_p^\nabla)\tilde{u}_n, (I - \tilde{\Pi}_p^\nabla)\tilde{u}_n) + S^K((\mathbf{I} - \mathbf{\Pi}_p^0)\boldsymbol{\sigma}_n, (\mathbf{I} - \mathbf{\Pi}_p^0)\boldsymbol{\sigma}_n) \right], \end{aligned} \quad (41)$$

and define global error estimator

$$\eta_{\text{eq}}^2 := \sum_{K \in \mathcal{T}_n} \eta_{\text{eq},K}^2. \quad (42)$$

3.2 Reliability

We deduce the following upper bound from (40):

$$\begin{aligned} &\|\mathbb{K}^{\frac{1}{2}}\nabla(\tilde{u} - \tilde{u}_n)\|_{0,\Omega}^2 + \|\mathbb{K}^{-\frac{1}{2}}(\boldsymbol{\sigma} - \boldsymbol{\sigma}_n)\|_{0,\Omega}^2 \\ &\leq 2(\|\mathbb{K}^{\frac{1}{2}}(\nabla\tilde{u}_n - \nabla\tilde{\Pi}_p^\nabla\tilde{u}_n)\|_{0,\Omega}^2 + \|\mathbb{K}^{\frac{1}{2}}\nabla\tilde{\Pi}_p^\nabla\tilde{u}_n + \mathbb{K}^{-\frac{1}{2}}\mathbf{\Pi}_p^0\boldsymbol{\sigma}_n\|_{0,\Omega}^2 + \|\mathbb{K}^{-\frac{1}{2}}(\mathbf{\Pi}_p^0\boldsymbol{\sigma}_n - \boldsymbol{\sigma}_n)\|_{0,\Omega}^2) \\ &\quad + 2 \int_{\Omega} (\tilde{u} - \tilde{u}_n - q_{p-1})(f - \Pi_{p-1}^0 f) \quad \forall q_{p-1} \in \mathcal{S}^{p-1,-1}(\Omega, \mathcal{T}_n). \end{aligned}$$

Set q_{p-1} as the piecewise L^2 projection of $u - \tilde{u}_n$ over \mathcal{T}_n . Using standard h - and p - approximation estimates, we deduce

$$\begin{aligned} \int_{\Omega} (\tilde{u} - \tilde{u}_n - q_{p-1})(f - \Pi_{p-1}^0 f) &\leq \sum_{K \in \mathcal{T}_n} \|\tilde{u} - \tilde{u}_n - q_{p-1}\|_{0,K} \|f - \Pi_{p-1}^0 f\|_{0,K} \\ &\leq \max_{K \in \mathcal{T}_n} c_B(K) \sum_{K \in \mathcal{T}_n} \frac{h_K}{p} |\tilde{u} - \tilde{u}_n|_{1,K} \|f - \Pi_{p-1}^0 f\|_{0,K} \\ &\leq \max_{K \in \mathcal{T}_n} c_B(K) |\tilde{u} - \tilde{u}_n|_{1,\Omega} \left(\sum_{K \in \mathcal{T}_n} \frac{h_K^2}{p^2} \|f - \Pi_{p-1}^0 f\|_{0,K}^2 \right)^{\frac{1}{2}}, \end{aligned}$$

where $c_B(K)$ is the positive constant appearing in the h - and p -approximation estimates of, e.g., [4, Lemma 4.5].

Young's inequality entails

$$\begin{aligned} &\int_{\Omega} (\tilde{u} - \tilde{u}_n - q_{p-1})(f - \Pi_{p-1}^0 f) \\ &\leq 4\varepsilon \left(\max_{K \in \mathcal{T}_n} c_B(K) \right)^2 |\tilde{u} - \tilde{u}_n|_{1,\Omega}^2 + \frac{1}{4\varepsilon} \sum_{K \in \mathcal{T}_n} \frac{h_K^2}{p^2} \|f - \Pi_{p-1}^0 f\|_{0,K}^2 \\ &\leq 4k_*^{-\frac{1}{2}}\varepsilon \left(\max_{K \in \mathcal{T}_n} c_B(K) \right)^2 \|\mathbb{K}^{\frac{1}{2}}\nabla(\tilde{u} - \tilde{u}_n)\|_{0,\Omega}^2 + \frac{1}{4\varepsilon} \sum_{K \in \mathcal{T}_n} \frac{h_K^2}{p^2} \|f - \Pi_{p-1}^0 f\|_{0,K}^2 \end{aligned}$$

for all $\varepsilon > 0$, where $c_B(K)$ denotes the best hp -approximation constant on element K .

Recalling (9) and setting

$$\varepsilon = \frac{k_*^{\frac{1}{2}}}{16(\max_{K \in \mathcal{T}_n} c_B(K))^2},$$

we obtain

$$\begin{aligned}
& \|\mathbb{K}^{\frac{1}{2}} \nabla(\tilde{u} - \tilde{u}_n)\|_{0,\Omega}^2 + \|\mathbb{K}^{-\frac{1}{2}}(\boldsymbol{\sigma} - \boldsymbol{\sigma}_n)\|_{0,\Omega}^2 \\
& \leq 4 \left(\|\mathbb{K}^{\frac{1}{2}}(\nabla \tilde{u}_n - \nabla \tilde{\Pi}_p^\nabla \tilde{u}_n)\|_{0,\Omega}^2 + \|\mathbb{K}^{\frac{1}{2}} \nabla \tilde{\Pi}_p^\nabla \tilde{u}_n + \mathbb{K}^{-\frac{1}{2}} \mathbf{\Pi}_p^0 \boldsymbol{\sigma}_n\|_{0,\Omega}^2 \right. \\
& \quad \left. + \|\mathbb{K}^{-\frac{1}{2}}(\mathbf{\Pi}_p^0 \boldsymbol{\sigma}_n - \boldsymbol{\sigma}_n)\|_{0,\Omega}^2 \right) + 16 \frac{(\max_{K \in \mathcal{T}_n} c_B(K))^2}{k_*^{\frac{1}{2}}} \sum_{K \in \mathcal{T}_n} \frac{h_K^2}{p^2} \|f - \Pi_{p-1}^0 f\|_{0,K}^2 \\
& \leq 4 \|\mathbb{K}^{\frac{1}{2}} \nabla \tilde{\Pi}_p^\nabla \tilde{u}_n + \mathbb{K}^{-\frac{1}{2}} \mathbf{\Pi}_p^0 \boldsymbol{\sigma}_n\|_{0,\Omega}^2 \\
& \quad + 4 \sum_{K \in \mathcal{T}_n} \max(\tilde{\alpha}_*^{-1}, \alpha_*^{-1}) \left[\tilde{S}^K((I - \tilde{\Pi}_p^\nabla) \tilde{u}_n, (I - \tilde{\Pi}_p^\nabla) \tilde{u}_n) + S^K((\mathbf{I} - \mathbf{\Pi}_p^0) \boldsymbol{\sigma}_n, (\mathbf{I} - \mathbf{\Pi}_p^0) \boldsymbol{\sigma}_n) \right] \\
& \quad + 16 \frac{(\max_{K \in \mathcal{T}_n} c_B(K))^2}{k_*^{\frac{1}{2}}} \sum_{K \in \mathcal{T}_n} \frac{h_K^2}{p^2} \|f - \Pi_{p-1}^0 f\|_{0,K}^2.
\end{aligned}$$

Eventually, (22) entails

$$\begin{aligned}
& \|\mathbb{K}^{\frac{1}{2}} \nabla(\tilde{u} - \tilde{u}_n)\|_{0,\Omega}^2 + \|\mathbb{K}^{-\frac{1}{2}}(\boldsymbol{\sigma} - \boldsymbol{\sigma}_n)\|_{0,\Omega}^2 \leq 4 \|\mathbb{K}^{\frac{1}{2}} \nabla \tilde{\Pi}_p^\nabla \tilde{u}_n + \mathbb{K}^{-\frac{1}{2}} \mathbf{\Pi}_p^0 \boldsymbol{\sigma}_n\|_{0,\Omega}^2 \\
& \quad + 4 \sum_{K \in \mathcal{T}_n} \max(\tilde{\alpha}_*^{-1}, \alpha_*^{-1}) \left(\tilde{S}^K((I - \tilde{\Pi}_p^\nabla) \tilde{u}_n, (I - \tilde{\Pi}_p^\nabla) \tilde{u}_n) + S^K((\mathbf{I} - \mathbf{\Pi}_p^0) \boldsymbol{\sigma}_n, (\mathbf{I} - \mathbf{\Pi}_p^0) \boldsymbol{\sigma}_n) \right) \\
& \quad + 16 \frac{(\max_{K \in \mathcal{T}_n} c_B(K))^2}{k_*^{\frac{1}{2}}} \sum_{K \in \mathcal{T}_n} \frac{h_K^2}{p^2} \|f - \text{div}(\boldsymbol{\sigma}_n)\|_{0,K}^2.
\end{aligned} \tag{43}$$

All the terms on the right-hand side are computable, with the exception of the oscillation of the right-hand side. This term can be approximated at any precision employing a sufficiently accurate quadrature formula.

We have proven the following reliability result.

Theorem 3.1. *Let assumptions (G1), (G2), (K), and (D) be valid. Let \tilde{u} , and u and $\boldsymbol{\sigma}$ be the solutions to (6) and (8), respectively, and let \tilde{u}_n , and u_n and $\boldsymbol{\sigma}_n$ be the solutions to (13) and (21), respectively. The following bound on the exact error in terms of the equilibrated error estimator and oscillation terms is valid:*

$$\begin{aligned}
& \|\mathbb{K}^{\frac{1}{2}} \nabla(\tilde{u} - \tilde{u}_n)\|_{0,\Omega}^2 + \|\mathbb{K}^{-\frac{1}{2}}(\boldsymbol{\sigma} - \boldsymbol{\sigma}_n)\|_{0,\Omega}^2 \\
& \leq 4 \sum_{K \in \mathcal{T}_n} \max(\tilde{\alpha}_*^{-1}, \alpha_*^{-1}) \eta_{\text{eq},K}^2 + 16 \frac{(\max_{K \in \mathcal{T}_n} c_B(K))^2}{k_*^{\frac{1}{2}}} \sum_{K \in \mathcal{T}_n} \frac{h_K^2}{p^2} \|f - \text{div}(\boldsymbol{\sigma}_n)\|_{0,K}^2.
\end{aligned} \tag{44}$$

Bound (44) is fully explicit in terms of h and p , where the p -dependence is also contained in the stabilization constants.

Remark 8. In the standard finite element setting, see, e.g., [18], the first term on the right-hand side of (43) reads

$$\|\mathbb{K}^{\frac{1}{2}} \nabla \tilde{u}_n + \mathbb{K}^{-\frac{1}{2}} \boldsymbol{\sigma}_n\|_{0,\Omega},$$

whereas the second and the third vanish. The fourth term is a higher-order oscillation term.

3.3 Efficiency

Here, we show an upper bound on local equilibrated error estimator $\eta_{\text{eq},K}$ (41) in terms of the exact error. In other words, we prove the efficiency of the local equilibrated error estimator.

First, we focus on the norm of the projected discrete solutions, i.e., the first term on the right-hand side of (41). For all polygons K , using (9) and the stability of orthogonal projectors, we

get

$$\begin{aligned}
\|\mathbb{K}^{\frac{1}{2}}\nabla\tilde{\Pi}_p^\nabla\tilde{u}_n + \mathbb{K}^{-\frac{1}{2}}\mathbf{\Pi}_p^0\boldsymbol{\sigma}_n\|_{0,K}^2 &\leq 2\left(\|\mathbb{K}^{\frac{1}{2}}\nabla\tilde{u} - \nabla\tilde{\Pi}_p^\nabla\tilde{u}_n\|_{0,K}^2 + \|\mathbb{K}^{-\frac{1}{2}}(\boldsymbol{\sigma} - \mathbf{\Pi}_p^0\boldsymbol{\sigma}_n)\|_{0,K}^2\right) \\
&\leq 4\left(\|\mathbb{K}^{\frac{1}{2}}(\nabla\tilde{u} - \nabla\tilde{\Pi}_p^\nabla\tilde{u})\|_{0,K}^2 + \|\mathbb{K}^{\frac{1}{2}}\nabla\tilde{\Pi}_p^\nabla(\tilde{u} - \tilde{u}_n)\|_{0,K}^2\right. \\
&\quad \left.+ \|\mathbb{K}^{-\frac{1}{2}}(\boldsymbol{\sigma} - \mathbf{\Pi}_p^0\boldsymbol{\sigma})\|_{0,K}^2 + \|\mathbb{K}^{-\frac{1}{2}}\mathbf{\Pi}_p^0(\boldsymbol{\sigma} - \boldsymbol{\sigma}_n)\|_{0,K}^2\right) \\
&\leq 4\left(\|\mathbb{K}^{\frac{1}{2}}(\nabla\tilde{u} - \nabla\tilde{\Pi}_p^\nabla\tilde{u})\|_{0,K}^2 + \|\mathbb{K}^{\frac{1}{2}}\nabla(\tilde{u} - \tilde{u}_n)\|_{0,K}^2\right. \\
&\quad \left.+ \|\mathbb{K}^{-\frac{1}{2}}(\boldsymbol{\sigma} - \mathbf{\Pi}_p^0\boldsymbol{\sigma})\|_{0,K}^2 + \|\mathbb{K}^{-\frac{1}{2}}(\boldsymbol{\sigma} - \boldsymbol{\sigma}_n)\|_{0,K}^2\right).
\end{aligned}$$

Next, we deal with the stabilization terms, i.e., the second and third terms on the right-hand side of (41). We begin with the stabilization term stemming from the discretization of the primal formulation:

$$\begin{aligned}
\tilde{S}^K((I - \tilde{\Pi}_p^\nabla)\tilde{u}_n, (I - \tilde{\Pi}_p^\nabla)\tilde{u}_n) &\leq \tilde{\alpha}^*\|\mathbb{K}^{\frac{1}{2}}\nabla(I - \tilde{\Pi}_p^\nabla)\tilde{u}_n\|_{0,K}^2 \\
&\leq 2\tilde{\alpha}^*\left[\|\mathbb{K}^{\frac{1}{2}}\nabla(\tilde{u} - \tilde{u}_n)\|_{0,K}^2 + \|\mathbb{K}^{\frac{1}{2}}\nabla(\tilde{u} - \tilde{\Pi}_p^\nabla\tilde{u})\|_{0,K}^2 + \|\mathbb{K}^{\frac{1}{2}}\nabla\tilde{\Pi}_p^\nabla(\tilde{u} - \tilde{u}_n)\|_{0,K}^2\right] \\
&\leq 4\tilde{\alpha}^*\|\mathbb{K}^{\frac{1}{2}}\nabla(\tilde{u} - \tilde{u}_n)\|_{0,K}^2 + 2\tilde{\alpha}^*\|\mathbb{K}^{\frac{1}{2}}\nabla(\tilde{u} - \tilde{\Pi}_p^\nabla\tilde{u})\|_{0,K}^2.
\end{aligned}$$

Analogously, we show an upper bound on the stabilization term stemming from the discretization of the dual formulation:

$$S^K((\mathbf{I} - \mathbf{\Pi}_p^0)\boldsymbol{\sigma}_n, (\mathbf{I} - \mathbf{\Pi}_p^0)\boldsymbol{\sigma}_n) \leq 4\alpha^*\|\mathbb{K}^{-\frac{1}{2}}(\boldsymbol{\sigma} - \boldsymbol{\sigma}_n)\|_{0,K}^2 + 2\alpha^*\|\mathbb{K}^{-\frac{1}{2}}(\boldsymbol{\sigma} - \mathbf{\Pi}_p^0\boldsymbol{\sigma})\|_{0,K}^2.$$

Collecting the three estimates, we get

$$\begin{aligned}
\eta_{\text{eq},K}^2 &= \|\mathbb{K}^{\frac{1}{2}}\nabla\tilde{\Pi}_p^\nabla\tilde{u}_n + \mathbb{K}^{-\frac{1}{2}}\mathbf{\Pi}_p^0\boldsymbol{\sigma}_n\|_{0,K}^2 \\
&\quad + \tilde{S}^K((I - \tilde{\Pi}_p^\nabla)\tilde{u}_n, (I - \tilde{\Pi}_p^\nabla)\tilde{u}_n) + S^K((\mathbf{I} - \mathbf{\Pi}_p^0)\boldsymbol{\sigma}_n, (\mathbf{I} - \mathbf{\Pi}_p^0)\boldsymbol{\sigma}_n) \\
&\leq 4(1 + \tilde{\alpha}^*)\|\mathbb{K}^{\frac{1}{2}}\nabla(\tilde{u} - \tilde{u}_n)\|_{0,K}^2 + 2(2 + \tilde{\alpha}^*)\|\mathbb{K}^{\frac{1}{2}}\nabla(\tilde{u} - \tilde{\Pi}_p^\nabla\tilde{u}_n)\|_{0,K}^2 \\
&\quad + 4(1 + \alpha^*)\|\mathbb{K}^{-\frac{1}{2}}(\boldsymbol{\sigma} - \boldsymbol{\sigma}_n)\|_{0,K}^2 + 2(2 + \alpha^*)\|\mathbb{K}^{-\frac{1}{2}}(\boldsymbol{\sigma} - \mathbf{\Pi}_p^0\boldsymbol{\sigma}_n)\|_{0,K}^2.
\end{aligned} \tag{45}$$

We have proven the following efficiency result.

Theorem 3.2. *Let assumptions (G1), (G2), (K), and (D) be valid. Let \tilde{u} , and u and $\boldsymbol{\sigma}$ be the solutions to (6) and (8), respectively, and \tilde{u}_n , and u_n and $\boldsymbol{\sigma}_n$ be the solutions to (13) and (21), respectively. The following upper bound on local equilibrated error estimator $\eta_{\text{eq},K}$ in terms of the local exact error and best local polynomial approximation terms is valid: for every $K \in \mathcal{T}_n$,*

$$\begin{aligned}
\eta_{\text{eq},K}^2 &\leq 4(1 + \tilde{\alpha}^*)\|\mathbb{K}^{\frac{1}{2}}\nabla(\tilde{u} - \tilde{u}_n)\|_{0,K}^2 + 2(2 + \tilde{\alpha}^*)\|\mathbb{K}^{\frac{1}{2}}\nabla(\tilde{u} - \tilde{\Pi}_p^\nabla\tilde{u}_n)\|_{0,K}^2 \\
&\quad + 4(1 + \alpha^*)\|\mathbb{K}^{-\frac{1}{2}}(\boldsymbol{\sigma} - \boldsymbol{\sigma}_n)\|_{0,K}^2 + 2(2 + \alpha^*)\|\mathbb{K}^{-\frac{1}{2}}(\boldsymbol{\sigma} - \mathbf{\Pi}_p^0\boldsymbol{\sigma}_n)\|_{0,K}^2.
\end{aligned} \tag{46}$$

Bound (46) is fully explicit in terms of h and p , where the p -dependence is also contained in the stabilization constants.

Remark 9. The case of variable degree of accuracy is dealt with by substituting p with a local p_K on each element K of \mathcal{T}_n . This is reflected in estimates (44) and (46), as well as in the definition of stabilizations (32) and (33). In the residual estimator setting it is mandatory to demand that neighbouring elements have comparable degree of accuracy, see [12, equation (4)]. This condition is not needed in the analysis contained in the present paper. \blacksquare

4 Numerical results

In this section, we introduce an adaptive algorithm and an hp -refinement strategy, in order to show the performance of the hypercircle method and to compare it with that of the residual a posteriori approach.

We ought to compare equilibrated error estimator η_{eq} in (42) with the exact error of the method; see the left-hand side of (44). However, since functions in virtual element spaces are not known in closed-form, but only through their degrees of freedom, we cannot compute the exact errors. Rather, we compare the equilibrated error estimator with the following computable approximation of the error: given solutions $\boldsymbol{\sigma}$, u , and $\boldsymbol{\sigma}_n$, u_n to mixed problem (8) and VEM (21), respectively, define the approximate error for mixed VEM (21) as

$$\left(\|\mathbb{K}^{\frac{1}{2}}(\nabla u - \nabla \tilde{\Pi}_p^\nabla u_n)\|_{0,\Omega}^2 + \|\mathbb{K}^{-\frac{1}{2}}(\boldsymbol{\sigma} - \boldsymbol{\Pi}_p^0 \boldsymbol{\sigma})\|_{0,\Omega}^2 \right)^{\frac{1}{2}}. \quad (47)$$

Approximate error (47) converges with the same h - and p - convergence rate as the exact error. To see this, it suffices to use arguments analogous to those, e.g., in [12, Section 5].

Since we will compare the performance of the equilibrated error estimator with that of the residual error estimator, we introduce a computable approximation of the error for the primal formulation as well: given solutions \tilde{u} and \tilde{u}_n to the primal problem (6) and VEM (13), respectively, define the approximate error for primal VEM (13) as

$$\|\mathbb{K}^{\frac{1}{2}}(\nabla \tilde{u} - \nabla \tilde{\Pi}_p^\nabla \tilde{u}_n)\|_{0,\Omega}. \quad (48)$$

Approximate error (48) converges with the same h - and p - convergence rate as the exact error $\|\mathbb{K}^{\frac{1}{2}}(\nabla u - \nabla u_n)\|_{0,\Omega}$; see, e.g., [8, Section 5].

As stabilizations for the primal and mixed formulation, we use those defined in (32) and (33), respectively. We fix shifted and scaled monomials [5, equation (4.4)] as a polynomial basis in the definition of internal degrees of freedom (10) for the primal formulation. As for the choice of polynomial bases for internal moments (16) and (17) of the mixed formulation, we use those described in [32, Proposition 2.1].

Remark 10. For high polynomial degrees, these choices of the polynomial bases are not the most effective. Rather, we ought to consider some sort of orthogonalization of the polynomial bases, as proposed in [39] for the primal formulation. Since this has not been investigated for the mixed formulation so far, we postpone the investigation of the effects of the choice of the polynomial bases on the performance of the method to future works. ■

4.1 Experiments on the theoretical and practical stabilizations

Before proceeding with the numerical experiments for the adaptive algorithm, we show that the p -version of the method converges optimally in terms of p . Moreover, we compare numerically the theoretical and practical stabilizations presented above. As for primal formulation stabilizations (23) and (32), this has already been investigated in [39, Section 2.2]. Indeed, the method works extremely similarly even with a high degree of accuracy.

As for mixed formulation stabilizations (25) and (33), we provide here numerical evidence that they deliver similar results. To this aim, consider a coarse mesh with some nonconvex elements, as that depicted in Figure 1 (left). With the p -version of mixed VEM (21), we approximate the exact smooth solution

$$u(x, y) = \sin(\pi x) \sin(\pi y) \quad \text{on } \Omega := (0, 1)^2. \quad (49)$$

In Figure 1 (right), we show the decay of error (47) versus the polynomial degree.

At the practical level, the two stabilizations deliver similar, indeed practically identical, results. Since the practical one is easier to implement and faster to run, we henceforth stick to it.

4.2 The test cases

We test the performance of the virtual element method and of the equilibrated error estimator on the following test cases.

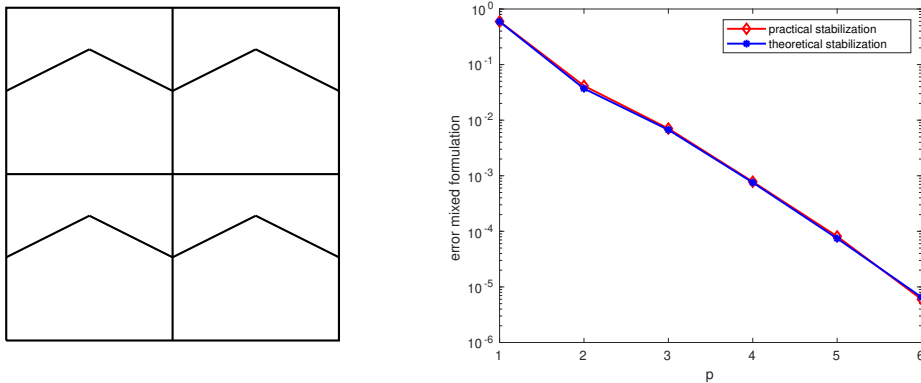


Figure 1: (Left panel:) a coarse mesh consisting of 8 elements, 4 of which being nonconvex. (Left panel:) the p -version of mixed VEM (21) applied to the exact solution in (49). We employ theoretical (25) and practical (33) stabilizations.

Test case 1. The first test case is defined on the L-shaped domain

$$\Omega_1 = (-1, 1) \setminus \{[0, 1) \times (-1, 0]\}.$$

In polar coordinates centred at $(0, 0)$, the solution to this problem reads

$$u_1(r, \theta) = r^{\frac{2}{3}} \sin\left(\frac{2}{3}\theta\right). \quad (50)$$

The primal formulation of the problem we are interested in is such that we have: zero Dirichlet boundary conditions on the edges generating the re-entrant corner; suitable Neumann boundary conditions on all the other edges; $\mathbb{K} = 1$; zero right-hand side, since u_1 is harmonic.

Test case 2. The second test case is defined on the slit domain

$$\Omega_2 := (-1, 1)^2 \setminus \{[0, 1) \times \{0\}\}.$$

In polar coordinates centred at $(0, 0)$, the solution to this problem reads

$$u_2(r, \theta) = r^{\frac{1}{4}} \sin\left(\frac{1}{4}\theta\right). \quad (51)$$

The primal formulation of the problem we are interested in is such that we have: suitable Neumann boundary conditions on the bottom edge of the slit; Dirichlet boundary conditions on all the other edges; $\mathbb{K} = 1$; zero right-hand side, since u_2 is harmonic. Note that the slit consists of two boundary edges: the bottom and the upper part of the slit.

We depict the solutions to the two test cases in Figure 2.

The remainder of the section is organized as follows. In Section 4.3, we recall the residual virtual element error estimator from [12]. Section 4.4 is devoted to analyze the behaviour of the efficiency index for the p -version of VEM, when using the residual and the equilibrated error estimators. The adaptive algorithm and the hp -refinements are described in Section 4.5, whereas the performance of the hp -adaptive algorithm is analyzed in Section 4.6.

4.3 The residual error estimator

In this section, we recall the residual error estimator derived in [12, Section 4] for the hp -version of the virtual element method and its properties. We assume that the diffusion coefficient \mathbb{K} is equal to 1, since this was the instance considered in [12].

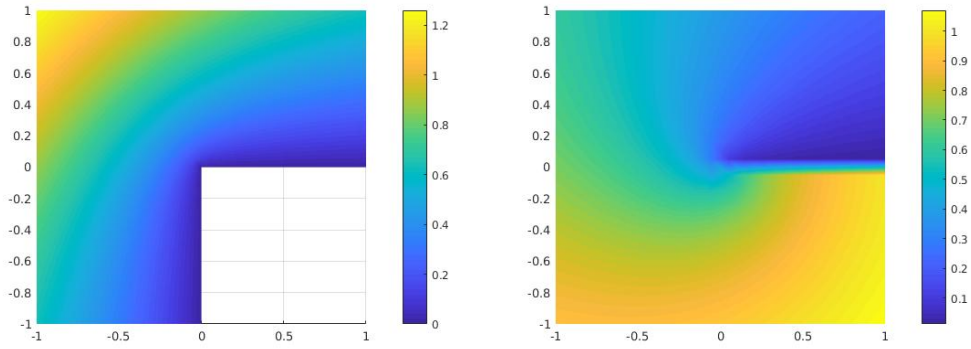


Figure 2: Test cases. (Left panel:) u_1 defined in (50). (Right panel:) u_2 defined in (51).

Given a mesh \mathcal{T}_n and a distribution of degrees of accuracy as in Remarks 3 and 5, introduce the following local residual error estimators: given solution \tilde{u}_n to (13), for all $K \in \mathcal{T}_n$,

$$\begin{aligned} \eta_{\text{res},K}^2 := & \frac{h_K^2}{p^2} \|\Delta \tilde{\Pi}_p^\nabla \tilde{u}_n + \tilde{\Pi}_{p-2}^0 f\|_{0,K}^2 + \frac{1}{2} \sum_{e \in \mathcal{E}^K, e \notin \Gamma_D} \frac{h_K}{p} \left\| \left[\mathbf{n}_e \cdot \nabla \tilde{\Pi}_p^\nabla \tilde{u}_n \right] \right\|_{0,e}^2 \\ & + S^K ((I - \tilde{\Pi}_p^\nabla) \tilde{u}_n, (I - \tilde{\Pi}_p^\nabla) \tilde{u}_n). \end{aligned}$$

The global residual error estimator is defined as

$$\eta_{\text{res}}^2 := \sum_{K \in \mathcal{T}_n} \eta_{\text{res},K}^2. \quad (52)$$

In [12, Theorem 1], the authors proved lower and upper bounds of the residual error estimator in terms of the error of the primal formulation. Although such bounds are optimal in terms of the mesh size, they are suboptimal in terms of the degree of accuracy of the method. This resembles what happens in the finite element method framework; see [40, Theorem 3.6]. The suboptimality is due to the use of polynomial inverse estimates when proving the efficiency.

4.4 Efficiency index: residual versus equilibrated error estimators

The aim of the present section is to investigate the behaviour of the efficiency indices of residual (52) and equilibrated (42) error estimators. In particular, we demonstrate the numerical p -robustness of the latter.

We define the efficiency index of the two error estimators as follows:

$$\begin{aligned} I_{\text{eq}}^2 &:= \frac{\eta_{\text{eq}}^2}{\|\mathbb{K}^{\frac{1}{2}} (\nabla u - \nabla \tilde{\Pi}_p^\nabla u_n)\|_{0,\Omega}^2 + \|\mathbb{K}^{-\frac{1}{2}} (\boldsymbol{\sigma} - \mathbf{\Pi}_p^0 \boldsymbol{\sigma})\|_{0,\Omega}^2}, \\ I_{\text{res}}^2 &:= \frac{\eta_{\text{res}}^2}{\|\mathbb{K}^{\frac{1}{2}} (\nabla \tilde{u} - \nabla \tilde{\Pi}_p^\nabla \tilde{u}_n)\|_{0,\Omega}^2}. \end{aligned} \quad (53)$$

We run the p -version of the method with exact solution u_1 defined in (50). As an underlying mesh, we fix a uniform Cartesian mesh with 12 elements. The behaviour of efficiency indices (53) is depicted in Figure 3.

From Figure 3, we observe that the efficiency index for the hypercircle method seems to be independent of p , differently from that of the residual error estimator. On the one hand, this is in partial accordance with bounds (43) and (45). Here, no polynomial inverse estimates have been used. On the other hand, the bounds depend on the stability constants of the method. As shown in (24) and (28), the stability constants might depend on p . Notwithstanding, it seems that such bounds are crude, and the stability constants do not play a role in terms of p . We performed analogous experiments on test case u_2 , and we obtained comparable results, which we omit for the sake of brevity. Eventually, note that the efficiency index for the equilibrated error estimator is close to 1.

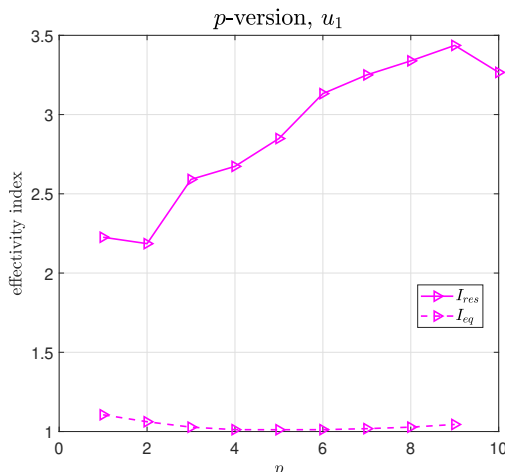


Figure 3: Effectivity indices I_{res} and I_{eq} (53) for the p -version of the method, using residual η_{res} (52) and equilibrated η_{eq} (42) error estimators. We consider the exact solution u_1 in (50) and use a uniform Cartesian mesh consisting of 12 elements.

4.5 The adaptive algorithm and hp -adaptive mesh refinements

In this section, we recall the structure of an adaptive algorithm, the meaning of h - and p -refinement, and how to choose between h - and p -refinements. The standard structure of an adaptive algorithm is

SOLVE \longrightarrow **ESTIMATE** \longrightarrow **MARK** \longrightarrow **REFINE.**

The remainder of this section is devoted to address the *marking* and *refining* steps. The latter consists in deciding whether to refine a marked element either in h or in p . Refining in p , the local space on an element K means that local degree of accuracy p_K on K is increased by one. The design of the global space and of its degrees of freedom is performed accordingly to Remarks 3 and 5.

We describe the h -refinement in more details. Firstly, we anticipate that we will employ Cartesian and triangular meshes, only. This might seem idiosyncratic, as we claimed that we want an adaptive method working on general meshes. However, the flexibility in employing polygons is exploited when refining squares or triangles and creating hanging nodes. In the refining procedure, we define a geometric square as a geometrical entity with four straight edges. For instance, a polygon with five vertices and having two adjacent edges on the same line is a geometric square. Analogously, we define a geometric triangle as a geometrical entity with three straight edges. A geometric square is refined into four smaller geometric squares by connecting its centroid to the midpoints of the four straight edges; see Figure 4 (left). Instead, a geometric triangle is refined into four smaller geometric triangles as in Figure 4 (right).

Observe that h -refinements of Cartesian and triangular meshes lead to meshes always consisting of geometric squares and triangles, respectively. Note that a refinement in presence of a hanging node in the proper place for the h -refinement is not creating an additional node.

We are left with the description of the marking strategy. Firstly, we describe how to choose the elements to mark. Secondly, we set a way to decide whether to mark for h - or p -refinement. Marking elements is a rather standard procedure. We mark for refinement all the elements $K \in \mathcal{T}_n$ such that, given a positive parameter $\sigma \in (0, 1)$,

$$\eta_{eq,K} \geq \sigma \overline{\eta_{eq}} := \sigma \frac{\eta_{eq}}{\text{card}(\mathcal{T}_n)}.$$

As far as the h - or p -marking is concerned, we could use several strategies; see for instance survey paper [41]. In words, the idea behind this choice resides in refining the mesh on the marked elements, where the solution is expected to be singular. An increase of the degree of accuracy is

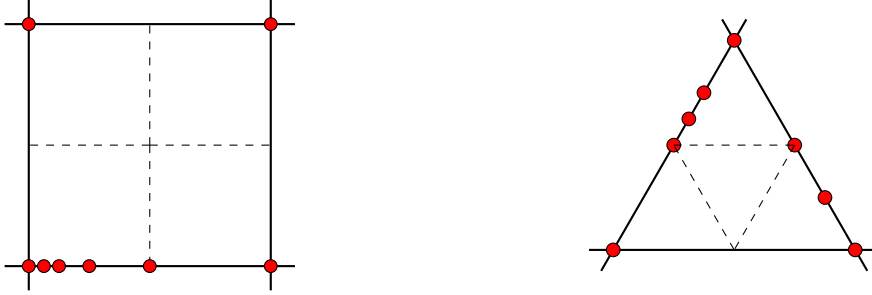


Figure 4: (*Left panel:*) Refining a geometric square with 8 vertices, 8 edges, and 4 straight edges. The refinement is performed by connecting the centroid to the midpoints of the four straight edges. (*Right panel:*) Refining a geometric triangle with 8 vertices, 8 edges, and 3 straight edges. The refinement is performed by subdividing the geometric triangle into 4 geometric subtriangles, with vertices given by the original vertices and the midpoints of the three straight edges. In red, we depict the vertices of the polygon under consideration.

performed on the marked elements, where the solution is expected to be smooth. Amongst the various techniques available in the literature, we follow the approach of Melenk and Wohlmuth, see [40, Section 4], which is based on comparing the actual equilibrated error estimator with a predicted one.

In the forthcoming numerical experiments, we set $\sigma = 1$, $\lambda = 0.2$, $\gamma_h = 1$, $\gamma_p = 1$, and $\gamma_n = 1$ in [40, Algorithm 4.4].

4.6 The h - and hp -adaptive algorithm

In this section, we present several numerical experiments on h - and hp -adaptivity employing the equilibrated error estimator in (42) and Melenk-Wohlmuth's refining strategy [40, Section 4]. We consider the two different test cases in (50)–(51), and compare the performance of the h -adaptive algorithm with $p = 1, 2$, and 3, and the hp -version of the method.

In Figures 5–6, we depict the performance of the h - (with $p = 1, 2$, and 3) and p -adaptive algorithm for all the test cases introduced in (50)–(51). We start with a coarse Cartesian mesh on the left and a coarse mesh made of structured triangles on the right.

We plot error (47) versus the cubic root of the number of degrees of freedom: we expect exponential convergence of the error in terms of the cubic root of the number of degrees of freedom, when employing an optimal hp -mesh. To see this, one has to combine the techniques in [8, 47].

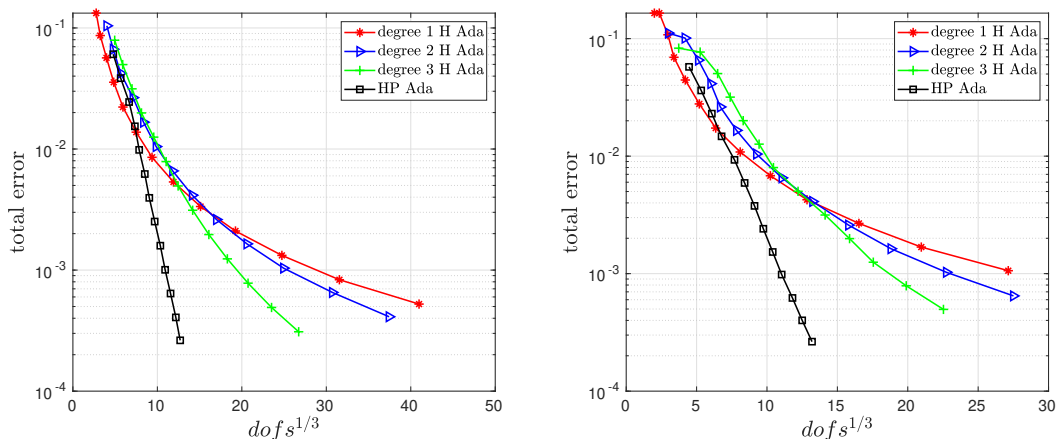


Figure 5: h - (with $p = 1, 2$, and 3) versus hp -adaptive algorithm. The solution is u_1 defined in (50). The starting mesh is (*left panel:*) a coarse Cartesian mesh and (*right panel:*) a coarse mesh of structured triangles.

From Figures 5–6, we observe the exponential decay of the error in terms of the cubic root of the number of degrees of freedom for hp -adaptive mesh refinements, and algebraic convergence

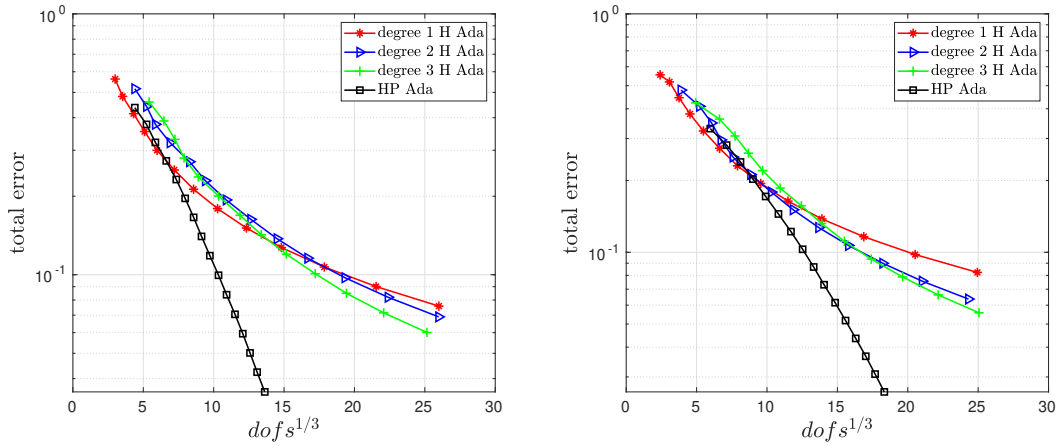


Figure 6: h - (with $p = 1, 2,$ and 3) versus hp -adaptive algorithm. The solution is u_2 defined in (51). The starting mesh is (*left panel:*) a coarse Cartesian mesh and (*right panel:*) a coarse mesh of structured triangles.

for h -adaptive refinement. The hp -adaptive version leads to smaller errors with fewer degrees of freedom compared to the h -adaptive version.

Finally, we exhibit the hp -meshes after 5 and 14 refinements of the adaptive algorithm for the Test Case 1; see Figure 7.

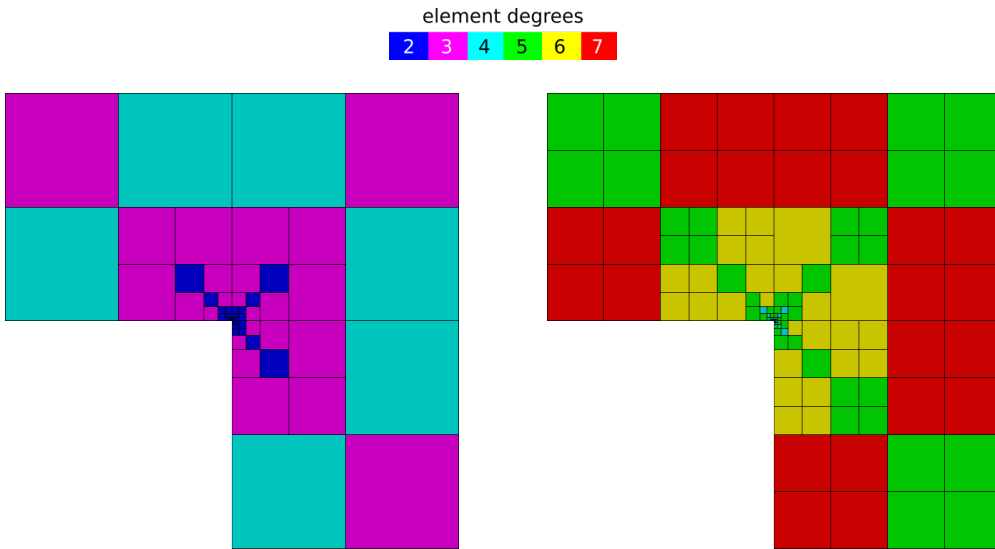


Figure 7: hp -adaptive algorithm. The solution is u_1 defined in (50). We exhibit blue hp -meshes after 5 (*left panel:*) and 14 (*right panel:*) refinements of the adaptive algorithm.

5 Local flux reconstruction in VEM: a first investigation

In Section 3, we proved lower and upper bounds of the exact error in terms of an equilibrated error estimator, where the dependence on the distribution of the degrees of accuracy is isolated within the stability constants. This is a major improvement compared to the results achieved in the residual error estimator setting; see [12, Theorem 1]. Nonetheless, the linear system associated with mixed discretization (21) has approximately three times the number of unknowns of the linear system associated with primal formulation (13). This downside can be overcome via the localization of the mixed VEM. This has been already investigated in several works within the continuous and discontinuous finite element framework; see [18] and [35], respectively, and the references therein.

In words, the localization technique works as follows. We construct an error estimator, which can be computed with the degrees of freedom of the solution to primal VEM (13) *and* those of another function, cheap to compute. Whilst in Section 3, this function was given by the solution to mixed VEM (21), here, it is provided by the combination of solutions to local mixed VEM, which are cheap to solve and can be parallelized.

The aim of this section is to provide an initial study towards the local flux reconstruction in VEM. We will be able to prove that the error estimator is reliable and satisfies a condition on equilibration of fluxes. However, we will not prove the efficiency. This is also reflected in the numerical results of Section 6.

Notation and assumptions. To simplify the forthcoming analysis, we henceforth assume

$$\mathbb{K} = 1, \quad \Gamma_D = \partial\Omega, \quad \Gamma_N = \emptyset.$$

We define the polygonal patch around a vertex $\nu \in \mathcal{V}_n$ and the elements of the mesh \mathcal{T}_n belonging to such patch as

$$\omega_\nu := \bigcup \{K \in \mathcal{T}_n \mid \nu \in \mathcal{V}^K\}, \quad \mathcal{T}_n^{\omega_\nu} = \{K \in \mathcal{T}_n \mid K \subset \omega_\nu\}.$$

Define the two following element spaces over the patch ω_ν :

$$\begin{aligned} V_n(\omega_\nu) &:= \mathcal{S}^{p-1, -1}(\omega_\nu, \mathcal{T}_n^{\omega_\nu}), \\ \Sigma_n(\omega_\nu) &:= \{\boldsymbol{\tau}_n \in H(\operatorname{div}, \omega_\nu) \mid \boldsymbol{\tau}_n|_K \in \Sigma_n(K) \quad \forall K \in \mathcal{T}_n^{\omega_\nu}, \llbracket \boldsymbol{\tau}_n \rrbracket_e = 0 \quad \forall e \in \mathcal{E}_n^I\}. \end{aligned}$$

We also define

$$\Sigma_{n,0}(\omega_\nu) := \{\boldsymbol{\tau}_n \in \Sigma_n(\omega_\nu) \mid \mathbf{n} \cdot \boldsymbol{\tau}_n = 0 \text{ on } \partial\omega_\nu\}, \quad V_n^*(\omega_\nu) := \left\{ v_n \in V_n(\omega_\nu) \mid \int_{\omega_\nu} v_n = 0 \right\}.$$

For each patch ω_ν , we introduce localized discrete bilinear form

$$a_n^{\omega_\nu}(\boldsymbol{\sigma}_n^\nu, \boldsymbol{\tau}_n^\nu) := \sum_{K \in \mathcal{T}_n^{\omega_\nu}} a_n^K(\boldsymbol{\sigma}_n^\nu, \boldsymbol{\tau}_n^\nu) \quad \forall \boldsymbol{\sigma}_n^\nu, \boldsymbol{\tau}_n^\nu \in \Sigma_n(\omega_\nu).$$

Construction of a virtual element partition of unity. We construct a virtual element partition of unity $\{\tilde{\varphi}_\nu\}_{\nu \in \mathcal{V}_n}$ associated with mesh \mathcal{T}_n by suitably fixing the degrees of freedom of each $\tilde{\varphi}_\nu$. To each vertex $\nu \in \mathcal{V}_n$, we associate a function $\tilde{\varphi}_\nu \in \tilde{V}_n$ defined through its degrees of freedom as follows. It is equal to 1 at ν , annihilates at all the other vertices, and is affine on the skeleton of the mesh.

For all $K \in \mathcal{T}_n$ with $\nu \in \mathcal{V}^K$, we proceed as follows. Let N^K be the number of vertices of K . Then, we set

$$\frac{1}{|K|} \int_K \tilde{\varphi}_\nu m_\alpha^K = \frac{1}{N^K |K|} \int_K m_\alpha^K \quad \forall |\alpha| = 0, \dots, p-2.$$

On all the elements $K \in \mathcal{T}_n$ such that ν is not a vertex of K , $\tilde{\varphi}_\nu$ is extended by 0.

Indeed, $\{\tilde{\varphi}_\nu\}_{\nu \in \mathcal{V}_n}$ is a partition of unity. To see this, define $\tilde{\varphi} = \sum_{\nu \in \mathcal{V}_n} \tilde{\varphi}_\nu$. The restriction of $\tilde{\varphi}$ on the skeleton of the mesh is equal to 1. Besides, the moments against piecewise polynomials up to degree $p-2$ are equal to the moments of the constant function 1. The unisolvency of the degrees of freedom of the primal virtual element space entails the assertion; see Section 2.2.

Such construction differs from the others in the VEM literature; see, e.g., [13, 45]. In these references, the partition of unity is defined on the skeleton of the mesh exactly as above. In the interior, each function is lifted to a harmonic function. The downside of this approach is that the internal moments are not known, although they are necessary for the computation of the various polynomial projectors.

Local flux reconstruction for interior patches. Now, we are in the position of defining the local VEM in mixed form. For all $\nu \in \mathcal{V}_n^I$, set

$$c^K = \frac{1}{|K|} \tilde{S}^K((I - \tilde{\Pi}_p^\nabla)\tilde{\varphi}_\nu, (I - \tilde{\Pi}_p^\nabla)\tilde{u}_n), \quad (54)$$

and consider the problem

$$\begin{cases} \text{find } (\boldsymbol{\sigma}_n^\nu, r_n^\nu) \in \boldsymbol{\Sigma}_{n,0}(\omega_\nu) \times V_n^*(\omega_\nu) \text{ such that, for all } \boldsymbol{\tau}_n^\nu \in \boldsymbol{\Sigma}_{n,0}(\omega_\nu) \text{ and } q_n^\nu \in V_n^*(\omega_\nu), \\ a_n^{\omega_\nu}(\boldsymbol{\sigma}_n^\nu, \boldsymbol{\tau}_n^\nu) - (\text{div}(\boldsymbol{\tau}_n^\nu), r_n^\nu)_{0,\omega_\nu} = - \sum_{K \in \mathcal{T}_n^{\omega_\nu}} (\tilde{\Pi}_{p-2}^0 \tilde{\varphi}_\nu \nabla \tilde{\Pi}_p^\nabla \tilde{u}_n, \mathbf{\Pi}_p^0 \boldsymbol{\tau}_n^\nu)_{0,K} \\ - (\text{div}(\boldsymbol{\sigma}_n^\nu), q_n^\nu)_{0,\omega_\nu} = - \sum_{K \in \mathcal{T}_n^{\omega_\nu}} (\tilde{\Pi}_{p-2}^0 \tilde{\varphi}_\nu f - \nabla \tilde{\Pi}_p^\nabla \tilde{\varphi}_\nu \cdot \nabla \tilde{\Pi}_p^\nabla \tilde{u}_n - c^K, q_n^\nu)_{0,K}. \end{cases} \quad (55)$$

Remark 11. The second equation in (55) represents the condition on equilibration of fluxes. This will become apparent in the sense of Lemma 5.1 below. On the other hand, the first equation in (55) is the residual equation. Roughly speaking, it is related to the fact that

$$\nabla r_n^\nu \approx \nabla \tilde{u}_n + \boldsymbol{\sigma}_n^\nu,$$

its weak formulation, and the VEM setting. The right-hand side of the first equation in (55) does not play a role in the proof of the reliability. However, it mimics the approach of, e.g., [35], where it plays an important role when proving the efficiency. \blacksquare

Thanks to definition (54), the second equation in (55) is valid also for functions without zero average. To see this, use that $\tilde{\varphi}_\nu$ is equal to 0 outside the patch ω_ν , and pick $q_n^\nu = 1$ in the second equation of (55), to get

$$\begin{aligned} 0 &= \int_{\partial\omega_\nu} \mathbf{n} \cdot \boldsymbol{\sigma}_n^\nu = \int_{\omega_\nu} \text{div}(\boldsymbol{\sigma}_n^\nu) \\ &= \sum_{K \in \mathcal{T}_n^{\omega_\nu}} \left(\int_K \left[\tilde{\Pi}_{p-2}^0 \tilde{\varphi}_\nu f - \nabla \tilde{\Pi}_p^\nabla \tilde{\varphi}_\nu \cdot \nabla \tilde{\Pi}_p^\nabla \tilde{u}_n \right] - \frac{1}{|K|} \tilde{S}^K((I - \tilde{\Pi}_p^\nabla)\tilde{\varphi}_\nu, (I - \tilde{\Pi}_p^\nabla)\tilde{u}_n)(1, 1)_{0,K} \right) \\ &= (\tilde{\Pi}_{p-2}^0 \tilde{\varphi}_\nu, f)_{0,\omega_\nu} - \sum_{K \in \mathcal{T}_n^{\omega_\nu}} \left((\nabla \tilde{\Pi}_p^\nabla \tilde{\varphi}_\nu, \nabla \tilde{\Pi}_p^\nabla \tilde{u}_n)_{0,K} + \tilde{S}^K((I - \tilde{\Pi}_p^\nabla)\tilde{\varphi}_\nu, (I - \tilde{\Pi}_p^\nabla)\tilde{u}_n) \right) \\ &= (\tilde{\Pi}_{p-2}^0 \tilde{\varphi}_\nu, f)_{0,\Omega} - \sum_{K \in \mathcal{T}_n} \left((\nabla \tilde{\Pi}_p^\nabla \tilde{\varphi}_\nu, \nabla \tilde{\Pi}_p^\nabla \tilde{u}_n)_{0,\Omega} + \tilde{S}^K((I - \tilde{\Pi}_p^\nabla)\tilde{\varphi}_\nu, (I - \tilde{\Pi}_p^\nabla)\tilde{u}_n) \right) \stackrel{(13)}{=} 0. \end{aligned} \quad (56)$$

For all $\nu \in \mathcal{V}_n$, problem (55) is well-posed. To see this, it suffices to use compatibility condition (56) together with Proposition 2.8, Remark 7, and the Babuška-Brezzi theory. The inf-sup condition can be proved as in Theorem 2.8.

Local flux reconstruction for boundary patches. We define the local mixed VEMs for boundary vertices in a slightly different fashion. Given $\nu \in \mathcal{V}_n^B$, set

$$\boldsymbol{\Sigma}_{n,0}^{\Gamma_D}(\omega_\nu) := \{ \boldsymbol{\tau}_n \in \boldsymbol{\Sigma}_n(\omega_\nu) \mid \mathbf{n}|_e \cdot \boldsymbol{\tau}_n = 0 \text{ for all } e \in \mathcal{E}_n^{\omega_\nu}, e \not\subset \Gamma_D \}.$$

We consider local VEMs of the following form:

$$\begin{cases} \text{find } (\boldsymbol{\sigma}_n^\nu, r_n^\nu) \in \boldsymbol{\Sigma}_{n,0}^{\Gamma_D}(\omega_\nu) \times V_n(\omega_\nu) \text{ such that, for all } \boldsymbol{\tau}_n^\nu \in \boldsymbol{\Sigma}_{n,0}^{\Gamma_D}(\omega_\nu) \text{ and } q_n^\nu \in V_n(\omega_\nu), \\ a_n^{\omega_\nu}(\boldsymbol{\sigma}_n^\nu, \boldsymbol{\tau}_n^\nu) - (\text{div}(\boldsymbol{\tau}_n^\nu), r_n^\nu)_{0,\omega_\nu} = - \sum_{K \in \mathcal{T}_n^{\omega_\nu}} (\tilde{\Pi}_{p-2}^0 \tilde{\varphi}_\nu \nabla \tilde{\Pi}_p^\nabla \tilde{u}_n, \mathbf{\Pi}_p^0 \boldsymbol{\tau}_n^\nu)_{0,K} \\ - (\text{div}(\boldsymbol{\sigma}_n^\nu), q_n^\nu)_{0,\omega_\nu} = - \sum_{K \in \mathcal{T}_n^{\omega_\nu}} (\tilde{\Pi}_{p-2}^0 \tilde{\varphi}_\nu f - \nabla \tilde{\Pi}_p^\nabla \tilde{\varphi}_\nu \cdot \nabla \tilde{\Pi}_p^\nabla \tilde{u}_n - c^K, q_n^\nu)_{0,K}. \end{cases} \quad (57)$$

To prove the well-posedness of problem (57), it suffices to use arguments similar to those employed in the proof of Theorem 2.8.

Next, define

$$\boldsymbol{\sigma}_n = \sum_{\nu \in \mathcal{V}_n} \boldsymbol{\sigma}_n^\nu, \quad (58)$$

and note that $\boldsymbol{\sigma}_n$ belongs to $\boldsymbol{\Sigma}_n$ by construction.

Lemma 5.1. *Let σ_n be defined as in (58). For all $K \in \mathcal{T}_n$, for all v_n in $V_n(K)$, i.e., for all v_n in $\mathbb{P}_{p-1}(K)$, the following identity is valid:*

$$\int_K \operatorname{div}(\sigma_n)v_n = \int_K f v_n. \quad (59)$$

Proof. Fix $K \in \mathcal{T}_n$. We have that

$$\sigma_n|_K = \sum_{\nu \in \mathcal{V}^K} \sigma_n^\nu.$$

Let $\nu \in \mathcal{V}^K$. Recall (56) entails that the second equation in (55) is valid for test functions without zero average. Pick q_n^ν equal to a polynomial v_n in K and zero elsewhere in the second equation of (55). Pick the same function in the second equation of (57) and deduce

$$\begin{aligned} \int_K \operatorname{div}(\sigma_n)v_n &= \sum_{\nu \in \mathcal{V}^K} \int_K \operatorname{div}(\sigma_n^\nu)v_n \\ &= \sum_{\nu \in \mathcal{V}^K} \{(\tilde{\Pi}_{p-2}^0 \tilde{\varphi}_\nu, f v_n)_{0,K} - (\nabla \tilde{\Pi}_p^\nabla \tilde{\varphi}_\nu, \nabla \tilde{\Pi}_p^\nabla u_n v_n)_{0,K} \\ &\quad - \frac{1}{|K|} (\tilde{S}^K((I - \tilde{\Pi}_p^\nabla) \tilde{\varphi}_\nu, (I - \tilde{\Pi}_p^\nabla) \tilde{u}_n), v_n)_{0,K}\}. \end{aligned}$$

Using that

$$\tilde{\Pi}_{p-2}^0 \left(\sum_{\nu \in \mathcal{V}^K} \tilde{\varphi}_\nu \right) = 1, \quad \nabla \tilde{\Pi}_p^\nabla \left(\sum_{\nu \in \mathcal{V}^K} \tilde{\varphi}_\nu \right) = 0, \quad (I - \tilde{\Pi}_p^\nabla) \left(\sum_{\nu \in \mathcal{V}^K} \tilde{\varphi}_\nu \right) = 0,$$

we get

$$\begin{aligned} \int_K \operatorname{div}(\sigma_n)v_n &= \int_K f v_n - \sum_{\nu \in \mathcal{V}^K} \left\{ \frac{1}{|K|} \left((\tilde{S}^K((I - \tilde{\Pi}_p^\nabla) \tilde{\varphi}_\nu, (I - \tilde{\Pi}_p^\nabla) \tilde{u}_n), v_n)_{0,K} \right) \right\} \\ &= \int_K f v_n - \frac{(1, v_n)_{0,K}}{|K|} \sum_{\nu \in \mathcal{V}^K} \tilde{S}^K((I - \tilde{\Pi}_p^\nabla) \tilde{\varphi}_\nu, (I - \tilde{\Pi}_p^\nabla) \tilde{u}_n) = \int_K f v_n, \end{aligned}$$

which is the assertion. \square

5.1 A new error estimator and its reliability

In this section, we show a result proving the reliability of an error estimator computed by means of function σ_n (58) as well as of the solution to primal discrete formulation (13).

For all $K \in \mathcal{T}_n$, introduce local flux reconstruction error estimators

$$\begin{aligned} \eta_{\text{flur},K}^2 &= S^K((\mathbf{I} - \mathbf{\Pi}_p^0)\sigma_n, (\mathbf{I} - \mathbf{\Pi}_p^0)\sigma_n) + \tilde{S}^K((I - \tilde{\Pi}_p^\nabla)\tilde{u}_n, (I - \tilde{\Pi}_p^\nabla)\tilde{u}_n) \\ &\quad + \|\mathbf{\Pi}_p^0 \sigma_n + \nabla \tilde{\Pi}_p^\nabla \tilde{u}_n\|_{0,\Omega}^2. \end{aligned}$$

We define global local flux reconstruction error estimator η_{flur} as

$$\eta_{\text{flur}}^2 = \sum_{K \in \mathcal{T}_n} \eta_{\text{flur},K}^2. \quad (60)$$

Theorem 5.2. *Let assumptions (G1), (G2), (K), and (D) be valid. Let \tilde{u} and \tilde{u}_n be the solutions to (6) and (13), respectively, and σ_n be defined as in (58). The following upper bound on the error of the primal formulation is valid:*

$$|\tilde{u} - \tilde{u}_n|_{1,\Omega}^2 \lesssim \left[\max_{K \in \mathcal{T}_n} (\max(\alpha_*^{-1}, \tilde{\alpha}_*^{-1})) \right] \eta_{\text{flur}}^2 + \sum_{K \in \mathcal{T}_n} \left(\frac{h_K^2}{p^2} \|f - \operatorname{div}(\sigma_n)\|_{0,K}^2 \right). \quad (61)$$

The hidden constant is independent of p .

Proof. For all $v \in H_0^1(\Omega)$, we have

$$\begin{aligned}
|\tilde{u} - \tilde{u}_n|_{1,\Omega} &= \sup_{v \in H_0^1(\Omega), |v|_{1,\Omega}=1} (\nabla(\tilde{u} - \tilde{u}_n), \nabla v)_{0,\Omega} \stackrel{(6)}{=} \sup_v \{(f, v)_{0,\Omega} - (\nabla \tilde{u}_n, \nabla v)_{0,\Omega}\} \\
&= \sup_v \{(f, v)_{0,\Omega} - (\nabla \tilde{u}_n, \nabla v)_{0,\Omega} - (\boldsymbol{\sigma}_n, \nabla v)_{0,\Omega} - (\operatorname{div}(\boldsymbol{\sigma}_n), v)_{0,\Omega}\} \\
&= \sup_v \{(f - \operatorname{div} \boldsymbol{\sigma}_n, v)_{0,\Omega} - (\boldsymbol{\sigma}_n + \nabla \tilde{u}_n, \nabla v)_{0,\Omega}\} \\
&=: \sup_v |A - B| \leq \sup_v \{|A| + |B|\}.
\end{aligned} \tag{62}$$

We prove an upper bound on the two terms on the right-hand side of (62) separately. We begin with the first one. Using Lemma 5.1 testing with v_n , the piecewise L^2 projector onto $\mathbb{P}_{p-1}(K)$, using hp -best polynomial approximation properties, and the ℓ^2 Cauchy-Schwarz inequality, we deduce

$$\begin{aligned}
A &= (f - \operatorname{div}(\boldsymbol{\sigma}_n), v)_{0,\Omega} \stackrel{(59)}{=} \sum_{K \in \mathcal{T}_n} (f - \operatorname{div}(\boldsymbol{\sigma}_n), v - v_n)_{0,K} \\
&\lesssim \left(\sum_{K \in \mathcal{T}_n} \frac{h_K^2}{p^2} \|f - \operatorname{div}(\boldsymbol{\sigma}_n)\|_{0,K}^2 \right)^{\frac{1}{2}} |v|_{1,\Omega}.
\end{aligned} \tag{63}$$

As for the upper bound on the second term on the right-hand side of (62), we observe that

$$\begin{aligned}
|B| &= |(\boldsymbol{\sigma}_n + \nabla \tilde{u}_n, \nabla v)_{0,\Omega}| \\
&\leq |(\boldsymbol{\sigma}_n - \boldsymbol{\Pi}_p^0 \boldsymbol{\sigma}_n, \nabla v)_{0,\Omega}| + |(\boldsymbol{\Pi}_p^0 \boldsymbol{\sigma}_n + \nabla \tilde{\Pi}_p^\nabla \tilde{u}_n, \nabla v)_{0,\Omega}| + |(\nabla \tilde{u}_n - \nabla \tilde{\Pi}_p^\nabla \tilde{u}_n, \nabla v)_{0,\Omega}| \\
&\leq \left(\|\boldsymbol{\sigma}_n - \boldsymbol{\Pi}_p^0 \boldsymbol{\sigma}_n\|_{0,\Omega} + \|\boldsymbol{\Pi}_p^0 \boldsymbol{\sigma}_n + \nabla \tilde{\Pi}_p^\nabla \tilde{u}_n\|_{0,\Omega} + \|\nabla \tilde{u}_n - \nabla \tilde{\Pi}_p^\nabla \tilde{u}_n\|_{0,\Omega} \right) |v|_{1,\Omega}.
\end{aligned}$$

Using the coercivity property of stabilizations (12) and (19), we get

$$\begin{aligned}
|B| &\leq \left(\sum_{K \in \mathcal{T}_n} \left[\alpha_*^{-1} S^K((\mathbf{I} - \boldsymbol{\Pi}_p^0) \boldsymbol{\sigma}_n, (\mathbf{I} - \boldsymbol{\Pi}_p^0) \boldsymbol{\sigma}_n) + \tilde{\alpha}_*^{-1} \tilde{S}^K((I - \tilde{\Pi}_p^\nabla) \tilde{u}_n, (I - \tilde{\Pi}_p^\nabla) \tilde{u}_n) \right]^{\frac{1}{2}} \right. \\
&\quad \left. + \|\boldsymbol{\Pi}_p^0 \boldsymbol{\sigma}_n + \nabla \tilde{\Pi}_p^\nabla \tilde{u}_n\|_{0,\Omega} \right) |v|_{1,\Omega}.
\end{aligned} \tag{64}$$

The assertion follows by plugging (63) and (64) in (62). \square

Theorem 5.2 shows the reliability of the local flux reconstruction error estimator. The second term on the right-hand side of (61) represents the oscillation in equilibrated flux condition (59).

5.2 Lack of efficiency

In this section, we give hints on why we are not able to prove the efficiency of error estimator (60) and why it is probably not valid in general.

To this aim, we first recall what happens in the finite element setting. Given the patch ω_ν consisting of triangles around an internal vertex ν , let $\mathbb{RT}_n(\omega_\nu)$ be the associated Raviart-Thomas space of order p . Moreover, let $Q_n(\omega_\nu)$ be the space of piecewise polynomials of degree p associated with the subtriangulation of ω_ν . Observe that partition of unity elements $\tilde{\varphi}_\nu$ are standard linear hat functions. The FEM counterpart of (55) reads

$$\left\{ \begin{array}{l} \text{find } (\boldsymbol{\sigma}_n^\nu, r_n^\nu) \in \mathbb{RT}_n(\omega_\nu) \times Q_n(\omega_\nu) \text{ such that, for all } \boldsymbol{\tau}_n^\nu \in \mathbb{RT}_n(\omega_\nu) \text{ and } q_n^\nu \in Q_n(\omega_\nu), \\ (\boldsymbol{\sigma}_n^\nu, \boldsymbol{\tau}_n^\nu)_{0,\omega_\nu} - (\operatorname{div}(\boldsymbol{\tau}_n^\nu), r_n^\nu)_{0,\omega_\nu} = -(\tilde{\varphi}_\nu \nabla \tilde{u}_n, \boldsymbol{\tau}_n^\nu)_{0,\omega_\nu} \\ -(\operatorname{div}(\boldsymbol{\sigma}_n^\nu), q_n^\nu)_{0,\omega_\nu} = -(\tilde{\varphi}_\nu f - \nabla \tilde{\varphi}_\nu \cdot \nabla \tilde{u}_n, q_n^\nu)_{0,\omega_\nu}. \end{array} \right. \tag{65}$$

The first step towards the proof of the local efficiency of the error estimator is based on an H^1 representation of the residual. In particular, introduce $r^\nu \in H^1(\omega_\nu) \setminus \mathbb{R}$ the solution to

$$(\nabla r^\nu, \nabla v)_{0,\omega_\nu} = -(\tilde{\varphi}_\nu \nabla \tilde{u}_n, \nabla v) + (\tilde{\varphi}_\nu f - \nabla \tilde{\varphi}_\nu \cdot \nabla \tilde{u}_n, v)_{0,\omega_\nu} \quad \forall v \in H^1(\omega_\nu) \setminus \mathbb{R}. \tag{66}$$

This equation is obtained by formally substituting v and ∇v to q_n^ν and τ_n^ν , using twice an integration by parts, and combining the two equations in (65).

As in [18, 26], the following bound can be proven:

$$|r^\nu|_{1, \omega_\nu} \lesssim |u - \tilde{u}_n|_{1, \omega_\nu}, \quad (67)$$

where the hidden constant depends on a Poincaré constant.

A crucial ingredient in the proof of (67) consists in observing that

$$\begin{aligned} -(\tilde{\varphi}_\nu \nabla \tilde{u}_n, \nabla v) + (\tilde{\varphi}_\nu f - \nabla \tilde{\varphi}_\nu \cdot \nabla \tilde{u}_n, v)_{0, \omega_\nu} &= (f, \tilde{\varphi}_\nu v)_{0, \omega_\nu} - (\nabla \tilde{u}_n, \nabla(\tilde{\varphi}_\nu v))_{0, \omega_\nu} \\ &= (\nabla(u - \tilde{u}_n), \nabla(\tilde{\varphi}_\nu v))_{0, \omega_\nu}. \end{aligned} \quad (68)$$

This is the first step towards the proof of the efficiency, as then it suffices to show that the error estimator is smaller than the energy of the H^1 residual. In what follows, we explain how the VEM counterpart of (66) looks like, and what are the issues in deriving estimates of the type in (67).

The main differences in the FE and VE approaches is that in the latter we have to deal with projectors, stabilizations, and functions that are not available in closed-form. We formally substitute v and ∇v to q_n^ν and τ_n^ν . Using the first equation in (55), we can write

$$\begin{aligned} &(\nabla r^\nu, \nabla v)_{0, \omega_\nu} \\ &= - \sum_{K \in \mathcal{T}_n^{\omega_\nu}} \left[(\tilde{\Pi}_{p-2}^0 \tilde{\varphi}_\nu \nabla \tilde{\Pi}_p^\nabla \tilde{u}_n, \mathbf{\Pi}_p^0 \nabla v)_{0, K} - a_n^K(\sigma_n^\nu, \nabla v) \right] \\ &= - \sum_{K \in \mathcal{T}_n^{\omega_\nu}} \left[(\tilde{\Pi}_{p-2}^0 \tilde{\varphi}_\nu \nabla \tilde{\Pi}_p^\nabla \tilde{u}_n, \mathbf{\Pi}_p^0 \nabla v)_{0, K} \underbrace{- a_n^K(\sigma_n^\nu, \nabla v) + a^K(\sigma_n^\nu, \nabla v)}_{=: A} - a^K(\sigma_n^\nu, \nabla v) \right]. \end{aligned} \quad (69)$$

Term A is a consistency error, which can be optimally approximated. Thence, we deal with the last term appearing on the right-hand side of (69). Using the definition of orthogonal projectors, an integration by parts, and the definition of the jumps, we get

$$-a^{\omega_\nu}(\sigma_n^\nu, \nabla v) = (\operatorname{div}(\sigma_n^\nu), v)_{0, \omega_\nu}.$$

Inserting this bound into (69) and using formally the second equation in (55) yield

$$\begin{aligned} &(\nabla r^\nu, \nabla v)_{0, \omega_\nu} \\ &= A + \sum_{K \in \mathcal{T}_n^{\omega_\nu}} \left[-(\tilde{\Pi}_{p-2}^0 \tilde{\varphi}_\nu \nabla \tilde{\Pi}_p^\nabla \tilde{u}_n, \mathbf{\Pi}_p^0 \nabla v)_{0, K} + (\tilde{\Pi}_{p-2}^0 \tilde{\varphi}_\nu f - \nabla \tilde{\Pi}_p^\nabla \tilde{\varphi}_\nu \cdot \nabla \tilde{\Pi}_p^\nabla \tilde{u}_n, v)_{0, K} \right]. \\ &= A - \underbrace{\sum_{K \in \mathcal{T}_n} (\nabla \tilde{\Pi}_p^\nabla \tilde{u}_n, \tilde{\Pi}_{p-2}^0 \tilde{\varphi}_\nu \mathbf{\Pi}_p^0 \nabla v + \nabla \tilde{\Pi}_p^\nabla \tilde{\varphi}_\nu v)_{0, K}}_{=: B} + \sum_{K \in \mathcal{T}_n} (f, \tilde{\Pi}_{p-2}^0 \tilde{\varphi}_\nu v)_{0, K}. \end{aligned}$$

Eventually, we analyze the last term on the right-hand side. Using the continuous problem (4) and an integration by parts lead us to

$$\sum_{K \in \mathcal{T}_n} (f, \tilde{\Pi}_{p-2}^0 \tilde{\varphi}_\nu v)_{0, K} = \sum_{K \in \mathcal{T}_n^{\omega_\nu}} (\nabla \tilde{u}, \nabla(\tilde{\Pi}_{p-2}^0 \tilde{\varphi}_\nu v))_{0, K} - \sum_{e \in \mathcal{E}_n^{\omega_\nu}} (u, \llbracket \tilde{\Pi}_{p-2}^0 \tilde{\varphi}_\nu v \rrbracket)_{0, e} =: C + D.$$

Combining all the above estimates, we arrive at

$$(\nabla r^\nu, \nabla v)_{0, \omega_\nu} = A + B + C + D.$$

In the FE setting the terms B and C are combined together, see (68). Here, this is not possible due to the presence of different projectors, which allow us to use neither the product rule nor the continuous formulation as in (68). Importantly, the culprit of the lack of efficiency is not the stabilization of the method nor the choice of the partition of unity. Rather, it is a mismatch in the use of the projections in the definition of local problems (55).

Indeed, in Section 6 below, we provide numerical evidence that the efficiency, in the current setting, is not valid.

6 Numerical results on the local flux reconstruction

In this section, we present some numerical results on the local flux reconstruction presented in Section 5. The aim is to show that reliability (61) and equilibrated flux condition (59) are valid. Interestingly, we will observe that the efficiency does not take place for the high-order VEM.

We consider the following test case.

Test case 3. Consider square domain $\Omega_3 = (0, 1)^2$ and the exact solution

$$u_3(x, y) = x(1 - x)y(1 - y). \quad (70)$$

The primal formulation of the problem we are interested in is such that we have: zero Dirichlet boundary conditions on the boundary edges; $\mathbb{K} = 1$; a right-hand side computed accordingly with (70).

We want to analyse the behaviour of following quantities:

- the error of the method $|u - u_n|_{1,\Omega}$;
- error estimator η_{flur} (60);
- the oscillation in the equilibrated flux condition, given by

$$\sqrt{\sum_{K \in \mathcal{T}_n} \left(\frac{h_K^2}{p^2} \|f - \text{div}(\sigma_n)\|_{0,K}^2 \right)}; \quad (71)$$

- the quantity

$$\sqrt{\sum_{\nu \in \mathcal{V}_n} \|\Pi_p^0 \sigma_n^\nu + \tilde{\Pi}_{p-2}^0 \tilde{\varphi}_\nu \nabla \tilde{\Pi}_p^\nabla \tilde{u}_n\|_{0,\omega_\nu}^2}. \quad (72)$$

We are interested in the performance of the h -version of the method for some values of degree of accuracy p . More precisely, in Section 6.1, we present the case $p = 1$, where we will also observe efficiency. Instead, in Section 6.2, we take $p = 2$ and show that we miss efficiency, albeit the equilibration of fluxes is valid, in accordance with the theoretical prediction of Lemma 5.1.

6.1 The case $p = 1$

In this section, we consider test case 3, with exact solution u_3 in (70), and study the performance of the h -version of the method with degree of accuracy $p = 1$ using uniform triangular and Cartesian meshes. Local problems (55) and (57) are extremely simplified for the lowest order case on triangular meshes. Indeed, the virtual element spaces with $p = 1$ on triangular meshes are standard finite element methods. Therefore, all the projectors and stabilizations disappear in the formulation.

In Tables 1 and 2, we depict the decay of the error of the method $|u - u_n|_{1,\Omega}$ with the corresponding experimentally determined order of convergence (EOC), error estimator η_{flur} (60), the oscillation in the equilibrated flux condition introduced in (71), and quantity (72), for uniform triangular and Cartesian meshes, respectively.

Table 1 h -version of the method using triangular meshes with degree of accuracy $p = 1$.

	$ u - u_n _{1,\Omega}$	EOC	η_{flur}	$\eta_{\text{flur}}/ u - u_n _{1,\Omega}$	(71)	(72)
mesh 1	0.446	—	0.469	1.0515	6.454e-02	7.784e-02
mesh 2	0.234	0.927	0.260	1.1121	1.638e-02	5.860e-02
mesh 3	0.120	0.966	0.137	1.1422	4.112e-03	5.104e-02
mesh 4	0.060	0.9872	0.071	1.1804	1.029-03	4.869e-02

Table 2 h -version of the method using uniform Cartesian meshes with degree of accuracy $p = 1$.

	$ u - u_n _{1,\Omega}$	EOC	η_{flux}	$\eta_{\text{flux}}/ u - u_n _{1,\Omega}$	(71)	(72)
mesh 1	0.339	—	0.362	1.068	1.035e-02	5.723e-02
mesh 2	0.169	0.999	0.186	1.098	1.638e-02	4.703e-02
mesh 3	0.084	0.999	0.093	1.106	2.600e-03	4.407e-02
mesh 4	0.042	0.999	0.046	1.108	6.507e-04	4.329e-02

From Table 1, we observe that the decay of the error is optimal and that error estimator η_{flux} is efficient. This could have been expected, since on triangular meshes and $p = 1$ the VEM coincides with the lowest order FEM, where it is well-known that the error estimator is reliable and efficient. Moreover, the oscillation in the equilibrated flux condition introduced in (71) is of higher order.

6.2 The case $p = 2$

In this section, we consider test case 3, with exact solution u_3 in (70), and study the performance of the h -version of the method with degree of accuracy $p = 2$ using uniform triangular and Cartesian meshes.

In Tables 3 and 4, we depict the decay of the error of the method $|u - u_n|_{1,\Omega}$ with the corresponding EOC, error estimator η_{flux} (60), the oscillation in the equilibrated flux condition introduced in (71), and quantity (72), for uniform triangular and Cartesian meshes, respectively.

Table 3 h -version of the method using triangular meshes with degree of accuracy $p = 2$.

	$ u - u_n _{1,\Omega}$	EOC	η_{flux}	$\eta_{\text{flux}}/ u - u_n _{1,\Omega}$	(71)	(72)
mesh 1	0.095	—	0.171	1.803	5.892e-03	5.105e-02
mesh 2	0.024	1.989	0.089	3.718	7.365e-04	4.722e-02
mesh 3	0.006	1.991	0.064	10.649	9.207e-05	4.614e-02
mesh 4	0.001	2	0.055	36.798	1.150e-05	4.588e-02

Table 4 h -version of the method using uniform Cartesian meshes with degree of accuracy $p = 2$.

	$ u - u_n _{1,\Omega}$	EOC	η_{flux}	$\eta_{\text{flux}}/ u - u_n _{1,\Omega}$	(71)	(72)
mesh 1	0.079	—	0.162	2.053	2.329e-03	5.518e-02
mesh 2	0.020	1.965	0.070	3.461	2.911e-04	5.130e-02
mesh 3	0.005	1.991	0.033	6.529	3.639e-05	5.027e-02
mesh 4	0.001	1.998	0.016	12.846	4.549e-06	5.000e-02

Differently from the low order case, in Tables 3 and 4, we observe a loss of efficiency of the method. This is in accordance with the arguments detailed in Section 5.2. Interestingly enough, in accordance with Section 5.1, the error estimator is however reliable and the oscillation in the equilibrated fluxes decay at high-order for both meshes.

6.3 The low order adaptive scheme

In this section, we consider test case 3, with exact solution u_3 in (70), and study the performance of the h -adaptive method with degree of accuracy $p = 1$ using a starting coarse triangular meshes. In Table 5, we depict the decay of the error of the method $|u - u_n|_{1,\Omega}$, error estimator η_{flux} (60), the oscillation in the equilibrated flux condition introduced in (71), and quantity (72).

Table 5 h -adaptive version of the method using a starting coarse triangular meshes with degree of accuracy $p = 1$.

	$ u - u_n _{1,\Omega}$	η_{flur}	$\eta_{\text{flur}}/ u - u_n _{1,\Omega}$	(71)	(72)
iteration 1	0.446	0.469	1.051	6.454e-02	7.784e-02
iteration 2	0.385	0.534	1.386	3.951e-02	7.813e-02
iteration 3	0.234	0.260	1.112	1.638e-02	5.860e-02
iteration 4	0.182	0.239	1.313	1.178e-02	6.102e-02
iteration 5	0.120	0.137	1.142	4.112e-03	5.104e-02
iteration 6	0.098	0.162	1.652	2.998e-03	5.517e-02
iteration 7	0.059	0.092	1.555	1.001e-03	5.045e-02
iteration 8	0.049	0.112	2.283	7.417e-04	5.238e-02

From Table 5, we observe a loss of efficiency for the error estimator. This is clear, owing to the fact that the adaptive refinement strategy produces nontriangular meshes, even starting with a uniform triangular mesh. Indeed, hanging nodes are added while performing the mesh refinement. Notwithstanding, we can still appreciate the reliability of the error estimator as well as the decay of the oscillation in the equilibrated fluxes.

6.4 The global version of (55)

In foregoing Sections 6.1 and 6.2, we observed that the error estimator is reliable, in accordance with the theoretical results of Section 5.1. However, as heuristically motivated in Section 5.2, we observed a lack of efficiency. To investigate better the effect of the mixed projectors appearing on the right-hand side of (55), we consider the global version of localized problem

$$\begin{cases} \text{find } (\boldsymbol{\sigma}_n^\nu, r_n^\nu) \in \boldsymbol{\Sigma}_n \times V_n \text{ such that, for all } \boldsymbol{\tau}_n^\nu \in \boldsymbol{\Sigma}_n \text{ and } q_n^\nu \in V_n, \\ a_n(\boldsymbol{\sigma}_n, \boldsymbol{\tau}_n) - (\text{div}(\boldsymbol{\tau}_n), r_n)_{0,\omega_\nu} = -(\nabla \tilde{\Pi}_p^\nabla \tilde{u}_n, \mathbf{\Pi}_p^0 \boldsymbol{\tau}_n)_{0,\Omega} \\ -(\text{div}(\boldsymbol{\sigma}_n), q_n)_{0,\omega_\nu} = -(f, q_n^\nu)_{0,\Omega} \end{cases} \quad (73)$$

and compute

$$\|r_n\|_{0,\Omega}, \quad \|\mathbf{\Pi}_p^0 \boldsymbol{\sigma}_n + \nabla \tilde{\Pi}_p^\nabla u_n\|_{0,\Omega}. \quad (74)$$

We expect that the two quantities (74) converge to zero. The first one represents the global residual, whereas the second one is the error on the projected flux reconstruction. For test case 3, we present the numerical results for the h -version of the method with uniform Cartesian meshes for degree $p = 2$ and 3 in Table 6.

Table 6 h -version of the global version (73) using a starting coarse uniform Cartesian meshes with degrees of accuracy $p = 2$ and $p = 3$.

	$p = 2, \ r_n\ _{0,\Omega}$	$\ \mathbf{\Pi}_p^0 \boldsymbol{\sigma}_n + \nabla \tilde{\Pi}_p^\nabla u_n\ _{0,\Omega}$	$p = 3, \ r_n\ _{0,\Omega}$	$\ \mathbf{\Pi}_p^0 \boldsymbol{\sigma}_n + \nabla \tilde{\Pi}_p^\nabla u_n\ _{0,\Omega}$
mesh 1	0.011	2.321e-02	1.766e-04	4.256e-04
mesh 2	0.002	3.920e-03	1.081e-05	2.896e-05
mesh 3	7.213e-4	6.695e-04	6.726e-07	1.913e-06
mesh 4	1.802e-4	1.166e-04	4.201e-08	1.308e-07
mesh 5	4.505e-05	2.07587e-05	2.626e-09	9.432e-09

Differently from the pure localized problem, we observe that the accuracy increases when increasing the order of the method. This is an additional confirmation that the main culprit for the lack of efficiency must be sought in the combination of different projection operators in the right-hand side of (55).

7 Conclusion

We presented the a posteriori error analysis for the virtual element method based on equilibrated fluxes. We introduced an equilibrated reliable and efficient a posteriori error estimator, using

the virtual element solutions to the primal and mixed formulations. Additionally, we showed that the discrete inf-sup constant for the mixed VEM is p -independent, and we constructed an explicit stabilization for the mixed VEM, characterized by lower and upper bounds with explicit dependence on the (local) degree of accuracy.

Several numerical experiments have been illustrated. On the one hand, we showed that the efficiency index for the hypercircle method is numerically p -independent. This is a major improvement with respect to the residual error estimator case. On the other hand, we discussed an hp -adaptive algorithm and we applied it to two test cases. We observed exponential convergence in terms of the cubic root of the number of degrees of freedom in all the test cases.

Eventually, we began the analysis of the localized flux reconstruction in VEM. Notably, we introduced a reliable computable error estimator, which can be obtained using the solution to the primal formulation and a combination of solutions to local mixed problems. Numerics showed that the equilibrium condition is fulfilled, but efficiency does not occur, with the exception of the low-order case. We also gave theoretical justifications for this lack of efficiency. It turns out that the culprit has to be sought neither in the stabilization nor in the definition of the partition of unity functions, but rather in the mismatch in the use of the projection operators appearing in the proposed local mixed VEM. In order to recover the efficiency of the localized method, suitable modifications to our approach will be the target of future works.

Acknowledgements. L. M. acknowledges the support of the Austrian Science Fund (FWF) project P33477.

References

- [1] P. F. Antonietti, S. Berrone, A. Borio, A. D’Auria, M. Verani, and S. Weisser. Anisotropic a posteriori error estimate for the virtual element method. <https://arxiv.org/abs/1904.10054>, 2020.
- [2] J. P. Aubin and H. G. Burchard. Some aspects of the method of the hypercircle applied to elliptic variational problems. In *Numerical Solution of Partial Differential Equations–II*, pages 1–67. Elsevier, 1971.
- [3] G. Auchmuty and J. C. Alexander. L^2 well-posedness of planar div–curl systems. *Arch. Ration. Mech. Anal.*, 160(2):91–134, 2001.
- [4] I. Babuška and M. Suri. The hp version of the finite element method with quasiuniform meshes. *ESAIM Math. Model. Numer. Anal.*, 21(2):199–238, 1987.
- [5] L. Beirão da Veiga, F. Brezzi, A. Cangiani, G. Manzini, L.D. Marini, and A. Russo. Basic principles of virtual element methods. *Math. Models Methods Appl. Sci.*, 23(01):199–214, 2013.
- [6] L. Beirão Da Veiga, F. Brezzi, L. D. Marini, and A. Russo. $H(\text{div})$ and $H(\text{curl})$ -conforming virtual element methods. *Numer. Math.*, 133(2):303–332, 2016.
- [7] L. Beirão da Veiga, F. Brezzi, L. D. Marini, and A. Russo. Mixed virtual element methods for general second order elliptic problems on polygonal meshes. *ESAIM Math. Model. Numer. Anal.*, 50(3):727–747, 2016.
- [8] L. Beirão da Veiga, A. Chernov, L. Mascotto, and A. Russo. Exponential convergence of the hp virtual element method with corner singularity. *Numer. Math.*, 138(3):581–613, 2018.
- [9] L. Beirão da Veiga, F. Dassi, and A. Russo. High-order virtual element method on polyhedral meshes. *Comput. Math. Appl.*, 74(5):1110–1122, 2017.
- [10] L. Beirão da Veiga, C. Lovadina, and A. Russo. Stability analysis for the virtual element method. *Math. Models Methods Appl. Sci.*, 27(13):2557–2594, 2017.
- [11] L. Beirão da Veiga and G. Manzini. Residual a posteriori error estimation for the virtual element method for elliptic problems. *ESAIM Math. Model. Numer. Anal.*, 49(2):577–599, 2015.
- [12] L. Beirão da Veiga, G. Manzini, and L. Mascotto. A posteriori error estimation and adaptivity in hp virtual elements. *Numer. Math.*, 143:139–175, 2019.
- [13] E. Benvenuti, A. Chiozzi, G. Manzini, and N. Sukumar. Extended virtual element method for the Laplace problem with singularities and discontinuities. *Comput. Methods Appl. Mech. Engrg.*, 356:571–597, 2019.
- [14] C. Bernardi, N. Fiétier, and R. G. Owens. An error indicator for mortar element solutions to the Stokes problem. *IMA J. Numer. Anal.*, 21(4):857–886, 2001.
- [15] S. Berrone and A. Borio. A residual a posteriori error estimate for the virtual element method. *Math. Models Methods Appl. Sci.*, 27(08):1423–1458, 2017.
- [16] S. Berrone, A. Borio, and F. Vicini. Reliable a posteriori mesh adaptivity in discrete fracture network flow simulations. *Comp. Methods Appl. Mech. Engrg.*, 354:904–931, 2019.
- [17] D. Boffi, F. Brezzi, and M. Fortin. *Mixed Finite Element Methods and Applications*, volume 44. Springer Series in Computational Mathematics, 2013.

- [18] D. Braess, V. Pillwein, and J. Schöberl. Equilibrated residual error estimates are p -robust. *Comput. Methods Appl. Mech. Engrg.*, 198(13-14):1189–1197, 2009.
- [19] D. Braess and J. Schöberl. Equilibrated residual error estimator for edge elements. *Math. Comp.*, 77(262):651–672, 2008.
- [20] S. C. Brenner and L.-Y.. Sung. Virtual element methods on meshes with small edges or faces. *Math. Models Methods Appl. Sci.*, 268(07):1291–1336, 2018.
- [21] F. Brezzi, R.S. Falk, and L.D. Marini. Basic principles of mixed virtual element methods. *Math. Mod. Num. Anal.*, 48(4):1227–1240, 2014.
- [22] A. Cangiani, E. H. Georgoulis, T. Pryer, and O. J. Sutton. A posteriori error estimates for the virtual element method. *Numer. Math.*, 137(4):857–893, 2017.
- [23] A. Cangiani, E. H. Georgoulis, and O. J. Sutton. Adaptive non-hierarchical Galerkin methods for parabolic problems with application to moving mesh and virtual element methods. <https://arxiv.org/abs/2005.05661>, 2020.
- [24] A. Cangiani and M. Munar. A posteriori error estimates for mixed virtual element methods. <https://arxiv.org/abs/1904.10054>, 2019.
- [25] S. Cao and L. Chen. Anisotropic error estimates of the linear virtual element method on polygonal meshes. *SIAM J. Numer. Anal.*, 56(5):2913–2939, 2018.
- [26] C. Carstensen and S. A. Funken. Fully reliable localized error control in the FEM. *SIAM J. Sci. Comput.*, 21(4):1465–1484, 1999.
- [27] T. Chaumont-Frelet, A. Ern, and M. Vohralík. On the derivation of guaranteed and p -robust a posteriori error estimates for the Helmholtz equation. https://hal.inria.fr/hal-02202233/file/chaumontfrelet_ern_vohralik_2019a.pdf, 2019.
- [28] H. Chi, L. Beirão da Veiga, and G. H. Paulino. A simple and effective gradient recovery scheme and a posteriori error estimator for the virtual element method. *Comput. Methods Appl. Mech. Engrg.*, 347:21–58, 2019.
- [29] S. Congreve, J. Gedicke, and I. Perugia. Robust adaptive hp discontinuous Galerkin finite element methods for the Helmholtz equation. *SIAM J. Sci. Comput.*, 41(2):A1121–A1147, 2019.
- [30] M. Costabel. A remark on the regularity of solutions of Maxwell’s equations on Lipschitz domains. *Math. Methods Appl. Sci.*, 12(4):365–368, 1990.
- [31] F. Dassi and L. Mascotto. Exploring high-order three dimensional virtual elements: bases and stabilizations. *Comput. Math. Appl.*, 75(9):3379–3401, 2018.
- [32] F. Dassi and G. Vacca. Bricks for the mixed high-order virtual element method: Projectors and differential operators. *Appl. Numer. Math.*, 155:140–159, 2020.
- [33] V. Dolejsi, A. Ern, and M. Vohralík. hp -adaptation driven by polynomial-degree-robust a posteriori error estimates for elliptic problems. *SIAM J. Sci. Comput.*, 38(5):A3220–A3246, 2016.
- [34] A. Ern, I. Smears, and M. Vohralík. Guaranteed, locally space-time efficient, and polynomial-degree robust a posteriori error estimates for high-order discretizations of parabolic problems. *SIAM J. Numer. Anal.*, 55(6):2811–2834, 2017.
- [35] A. Ern and M. Vohralík. Polynomial-degree-robust a posteriori estimates in a unified setting for conforming, nonconforming, discontinuous Galerkin, and mixed discretizations. *SIAM J. Numer. Anal.*, 53(2):1058–1081, 2015.
- [36] J. Gedicke, S. Geever, and I. Perugia. An equilibrated a posteriori error estimator for arbitrary-order Nédélec elements for magnetostatic problems. *J. Sci. Comput.*, 83(3), 2020.
- [37] H. Guo, C. Xie, and R. Zhao. Superconvergent gradient recovery for virtual element methods. *Math. Models Methods Appl. Sci.*, 29(11):2007–2031, 2019.
- [38] M. Křížek and P. Neittaanmäki. On the validity of Friedrichs’ inequalities. *Math. Scand.*, 54:17–26, 1984.
- [39] L. Mascotto. Ill-conditioning in the virtual element method: stabilizations and bases. *Numer. Methods Partial Differential Equations*, 34(4):1258–1281, 2018.
- [40] J. M. Melenk and B. I. Wohlmuth. On residual-based a posteriori error estimation in hp -FEM. *Adv. Comput. Math.*, 15(1-4):311–331, 2001.
- [41] W. F. Mitchell and M. A. McClain. A survey of hp -adaptive strategies for elliptic partial differential equations. In *Recent advances in computational and applied mathematics*, pages 227–258. Springer, 2011.
- [42] P. Monk. *Finite Element Methods for Maxwell’s Equations*. Oxford University Press, 2003.
- [43] D. Mora and G. Rivera. A priori and a posteriori error estimates for a virtual element spectral analysis for the elasticity equations. *IMA J. Numer. Anal.*, 40(1):322–357, 2020.
- [44] D. Mora, G. Rivera, and R. Rodriguez. A posteriori error estimates for a virtual elements method for the Steklov eigenvalue problem. *Comput. Math. Appl.*, 74(9):2172–2190, 2017.
- [45] I. Perugia, P. Pietra, and A. Russo. A plane wave virtual element method for the Helmholtz problem. *ESAIM Math. Model. Numer. Anal.*, 50(3):783–808, 2016.
- [46] W. Prager and J. L. Synge. Approximations in elasticity based on the concept of function space. *Quart. Appl. Math.*, 5(3):241–269, 1947.

- [47] D. Schötzau and T. P. Wihler. Exponential convergence of mixed hp -DGFEM for Stokes flow in polygons. *Numer. Math.*, 96(2):339–361, 2003.
- [48] I. Smears and M. Vohralík. Simple and robust equilibrated flux a posteriori estimates for singularly perturbed reaction–diffusion problems. *ESAIM Math. Model. Numer. Anal.*, 54(6):1951–1973, 2020.
- [49] H. Triebel. *Interpolation theory, function spaces, differential operators*. North-Holland, 1978.
- [50] S. Weißer. Anisotropic polygonal and polyhedral discretizations in finite element analysis. *ESAIM Math. Model. Numer. Anal.*, 53(2):475–501, 2019.